Cell Metabolism
Article

# Estradiol Regulates Brown Adipose Tissue Thermogenesis via Hypothalamic AMPK

Pablo B. Martínez de Morentin,[1,2] Ismael González-García,[1,2] Luís Martins,[1,2] Ricardo Lage,[1,2] Diana Fernández-Mallo,[1,2] Noelia Martínez-Sánchez,[1,2] Francisco Ruíz-Pino,[2,3,4] Ji Liu,[5,6,7] Donald A. Morgan,[8] Leonor Pinilla,[2,3,4] Rosalía Gallego,[9] Asish K. Saha,[10] Andries Kalsbeek,[5,6] Eric Fliers,[5] Peter H. Bisschop,[5] Carlos Diéguez,[1,2] Rubén Nogueiras,[1,2] Kamal Rahmouni,[8,11] Manuel Tena-Sempere,[2,3,4] and Miguel López[1,2,*]

[1]Department of Physiology, Research Center of Molecular Medicine and Chronic Diseases (CIMUS), University of Santiago de Compostela-Instituto de Investigación Sanitaria, Santiago de Compostela, 15782, Spain
[2]CIBER Fisiopatología de la Obesidad y Nutrición (CIBERobn), Santiago de Compostela, 15706, Spain
[3]Department of Cell Biology, Physiology and Immunology, University of Córdoba, Córdoba, 14004 Spain
[4]Instituto Maimónides de Investigación Biomédica (IMIBIC)/Hospital Universitario Reina Sofia (HURS), Córdoba, 14004, Spain
[5]Department of Endocrinology and Metabolism, Academic Medical Center (AMC), University of Amsterdam, Amsterdam, 1105 AZ, The Netherlands
[6]Department of Hypothalamic Integration Mechanisms, Netherlands Institute of Neuroscience (NIN), an Institute of the Royal Netherlands Academy of Arts and Science, Amsterdam, 1105 BA, The Netherlands
[7]Key Laboratory of Brain Function and Diseases, School of Life Sciences, University of Science and Technology of China, Chinese Academy of Sciences, Hefei, Anhui, 230026, P. R. China
[8]Department of Pharmacology, University of Iowa, Iowa City, IA 52242, USA
[9]Department of Morphological Sciences, School of Medicine, University of Santiago de Compostela, Santiago de Compostela, 15782, Spain
[10]Diabetes Research Unit, EBRC-827, Boston Medical Center, Boston, MA 02118, USA
[11]Department of Internal Medicine, University of Iowa, Iowa City, IA 52242, USA
*Correspondence: m.lopez@usc.es
http://dx.doi.org/10.1016/j.cmet.2014.03.031

## SUMMARY

**Estrogens play a major role in the modulation of energy balance through central and peripheral actions. Here, we demonstrate that central action of estradiol (E2) inhibits AMP-activated protein kinase (AMPK) through estrogen receptor alpha (ERα) selectively in the ventromedial nucleus of the hypothalamus (VMH), leading to activation of thermogenesis in brown adipose tissue (BAT) through the sympathetic nervous system (SNS) in a feeding-independent manner. Genetic activation of AMPK in the VMH prevented E2-induced increase in BAT-mediated thermogenesis and weight loss. Notably, fluctuations in E2 levels during estrous cycle also modulate this integrated physiological network. Together, these findings demonstrate that E2 regulation of the VMH AMPK-SNS-BAT axis is an important determinant of energy balance and suggest that dysregulation in this axis may account for the common changes in energy homeostasis and obesity linked to dysfunction of the female gonadal axis.**

## INTRODUCTION

Ovarian estrogens play a major role in the regulation of energy homeostasis (Gao and Horvath, 2008; Hill et al., 2013; Mauvais-Jarvis et al., 2013). Decreased levels of estradiol (E2) after menopause or ovariectomy (OVX) are also associated with hyperphagia, reduced energy expenditure, and weight gain (Rogers et al., 2009; Mauvais-Jarvis et al., 2013). In turn, E2 replacement therapy prevents OVX-induced obesity by decreasing feeding and increasing energy expenditure (Gao and Horvath, 2008; Finan et al., 2012; Mauvais-Jarvis et al., 2013). Likewise, hormone replacement therapy reverses the development of obesity and metabolic dysfunctions in postmenopausal women (Wren, 2009; Mauvais-Jarvis et al., 2013). Studies have also suggested variations in meal size and body weight in rats depending on the stage of the estrous cycle (Tritos et al., 2004), as well as during pregnancy and lactation (García et al., 2003).

Genetic models of loss of function of estrogen receptors (ERs), which are widely expressed in the hypothalamus (Shughrue et al., 1997), have demonstrated that mice with global or brain-specific targeted disruption of ER alpha (ERα) are obese, as a consequence of hyperphagia and hypometabolism (Heine et al., 2000; Xu et al., 2011). Similarly, mice and patients deficient for the aromatase enzyme, which mediates the conversion of androgens to estrogens, develop obesity (Grumbach and Auchus, 1999; Jones et al., 2000; Jones et al., 2001). Interestingly, estrogens display a nucleus-specific action within the hypothalamus to modulate energy balance, particularly within the arcuate (ARC) and ventromedial (VMH) nuclei. VMH-specific delivery of adeno-associated viral vectors silencing ERα in mice and rats leads to marked obesity, impaired glucose tolerance, and reduced energy expenditure (Musatov et al., 2007). Of note, these genetic manipulations did not alter food intake, indicating that estrogens actions in the VMH modulate specifically energy expenditure. In keeping with this, female mice lacking ERα in hypothalamic steroidogenic factor-1 (SF1) neurons of the VMH exhibit reduced energy expenditure and brown adipose tissue (BAT)-mediated thermogenesis, leading to obesity,

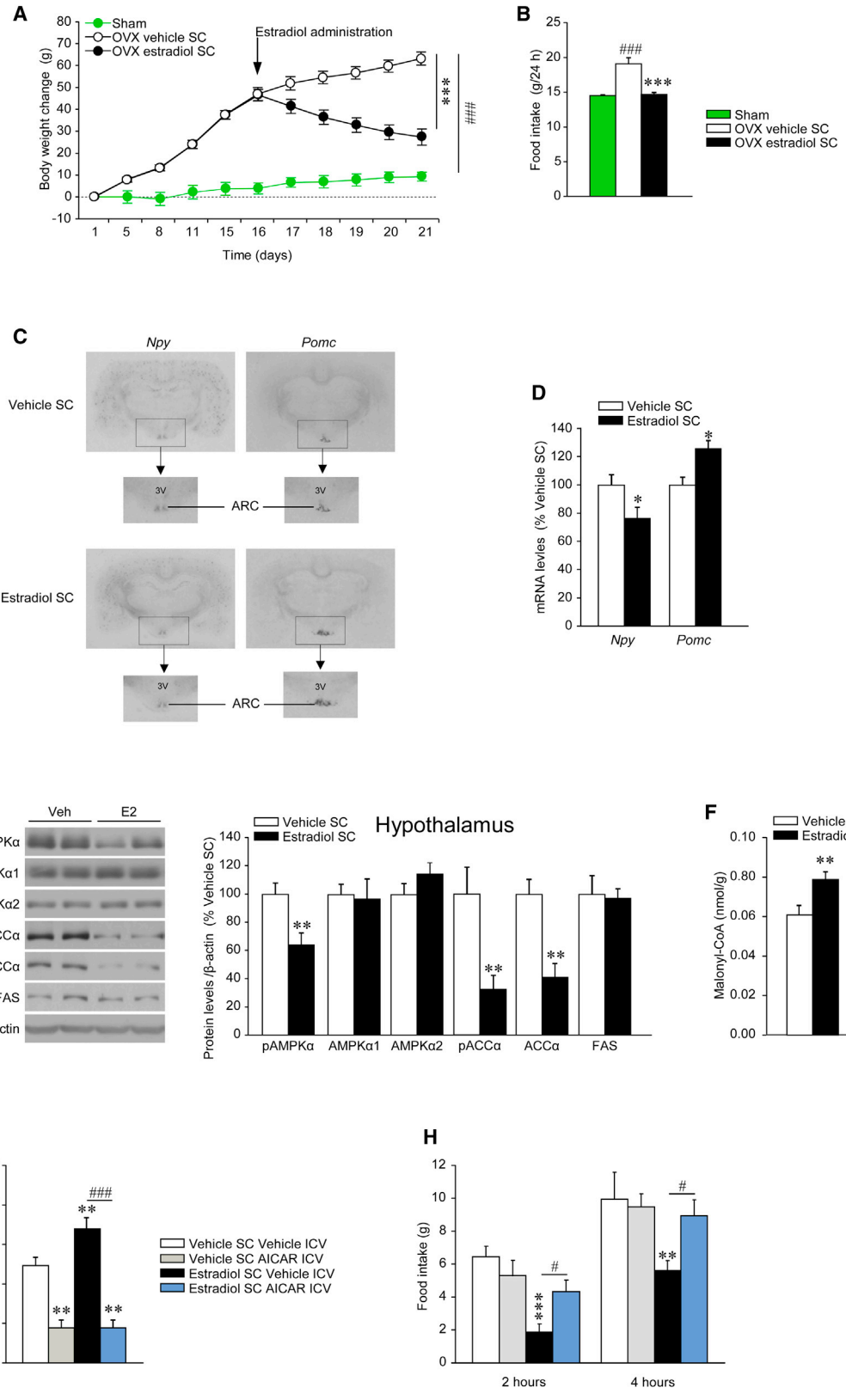


*(legend on next page)*

despite normal feeding (Xu et al., 2011). In contrast, deletion of ERα in proopiomelanocortin (POMC) neurons of the ARC leads to hyperphagia without changes in energy expenditure (Xu et al., 2011). Finally, concomitant deletion of ERα from both SF1 and POMC neurons recapitulates both phenotypes, causing hypometabolism, hyperphagia, and severe obesity (Xu et al., 2011).

Despite this evidence, the molecular and cellular events mediating E2-induced negative energy balance and BAT thermogenesis remain elusive. Thus, the aim of this study was to investigate the hypothalamic mechanism mediating E2-induced thermogenesis. We show that central E2 regulates BAT thermogenesis through ERα and activation of the sympathetic nervous system (SNS) by modulating hypothalamic AMP-activated protein kinase (AMPK), specifically in the VMH.

## RESULTS

### Peripheral E2 Induces Negative Energy Balance

OVX rats gained significantly more weight and developed a marked hyperphagia (Figures 1A and 1B). Subcutaneous (SC) treatment of OVX rats with E2 induced a marked reduction in body weight and food intake (Figures 1A and 1B) leading to a state of negative energy balance (Figure S1A available online). OVX rats showed the expected increase in serum luteinizing hormone (LH) and decrease in circulating E2 levels (confirming the efficiency of the OVX procedure), while SC E2 treatment recover both parameters to physiological levels (Figures S1B and S1C). For this reason, and in order to avoid a possible interference of fluctuations of ovarian E2 production during the estrous cycle, we used OVX rats in all the experiments (with the exception of Figures 7 and S7A–S7C, where intact rats were used).

The anorectic effect of E2 was found to be associated with decreased NPY mRNA and increased POMC mRNA levels in the ARC of OVX rats treated with E2 (Figures 1C and 1D). E2-treated rats showed decreased phosphorylated levels of AMPKα (pAMPKα) and ACCα (pACCα, which is inactive when phosphorylated) in the whole hypothalamus (Figure 1E). Consistent with ACC activation, we found that E2 increased the hypothalamic malonyl-CoA levels (Figure 1F). To establish the functional dependence of E2's actions on hypothalamic AMPK and malonyl-CoA levels, we investigated whether pharmacological activation of central AMPK could reverse the anorectic effects of E2. Intracerebroventricular (ICV) administration of the AMPK activator AICAR decreased hypothalamic malonyl-CoA concentration (Figure 1G) and reversed the hypophagia observed in rats treated with E2 (Figure 1H).

### E2 Modulates the Thermogenic Program in BAT Independently of Food Intake

To dissect the relative contribution of the anorectic effect of E2 to its impact on energy homeostasis, a group of vehicle-treated pair-fed rats (i.e., received the average amount of food eaten by the E2-treated rats the day before) was studied. SC administration of E2 to OVX rats decreased body weight largely exceeding that of pair-fed OVX rats, indicating a food-independent weight loss (Figures 2A and 2B). SC administration of E2 increased the mRNA expression or protein content of thermogenic markers, such as uncoupling protein-1 (UCP1), peroxisome-proliferator-activated receptor-gamma coactivator 1 alpha (PGC1α) and beta (PGC1β) in the BAT (Figures 2C and 2D), while no changes in browning markers (Waldén et al., 2012; Ohno et al., 2012; Fisher et al., 2012) were detected in white adipose tissue (WAT) (Figure S2A). Peripheral administration of E2 induced a slight upregulation of the thermogenic program in liver but not in skeletal muscle (Figures S2B and S2C). No changes in inflammatory markers were detected in muscle either (Figure S2C).

Next, we examined the possibility that these effects of E2 are centrally mediated. We found that ICV administration of E2 induced weight loss that was significantly larger than that observed in OVX pair-fed animals (Figures 2E and 2F). Consistently, the mRNA expression or protein content of UCP1, PGC1α, and PGC1β was markedly increased in BAT of ICV E2-treated rats when compared to both vehicle-treated and pair-fed animals (Figures 2G and 2H), whereas no changes in browning markers were found in WAT (Figure S2D). No increase in the expression of thermogenic or inflammatory markers was detected in the liver or muscle after ICV E2 administration (Figures S2E and S2F).

### Central E2 Increases Energy Expenditure and SNS Activity and Inhibits Hypothalamic AMPK

ICV E2-treated (5 nmol) rats showed decreased weight (Figure 3A), anorexia (Figure 3B), as well as a significantly higher body temperature (Figure 3C) and energy expenditure (EE) (Figure 3D) associated with reduced respiratory quotient (RQ) (which indicates increased lipid mobilization; Figure 3E) and locomotor activity (LA) (Figure 3F), which overall promote a negative energy balance (Figure S3A). Notably, a single ICV administration of E2 caused a marked increase in BAT sympathetic nerve traffic recorded directly by microneurography (Figure 3G). ICV E2 also decreased AMPK activation in the mediobasal hypothalamus (MBH) (Figure 3H).

### Central E2 Induces BAT Thermogenesis through the SNS

In order to further investigate whether ICV E2-induced increase in thermogenic markers correlated with changes in BAT thermogenesis, we used thermographic imaging analysis (Martínez de Morentin et al., 2012; Whittle et al., 2012). Of note, a lower ICV E2 dosage was used in these experiments. A total of 1 nmol of ICV E2 induced a marked weight loss, anorexia, and an increase

**Figure 1. Effect of SC E2 on Energy Balance**

(A–F) (A) Body weight change, (B) daily food intake, (C) in situ hybridization autoradiographic images, (D) *Npy* and *Pomc* mRNA levels in the ARC, (E) western blot autoradiographic images (left panel) and hypothalamic levels of proteins of AMPK pathway (right panel), and (F) hypothalamic malonyl-CoA levels of OVX rats and OVX rats SC treated with vehicle or E2.

(G and H) (G) Hypothalamic malonyl-CoA levels and (H) food intake of OVX rats SC treated with vehicle or E2 and ICV treated with vehicle or AICAR. Error bars represent SEM; n = 8–16 animals per experimental group. 3V: third ventricle; *, ** and ***p < 0.05, 0.01, and 0.001 *vs*. OVX E2 SC or vehicle SC vehicle ICV; #p < 0.05 E2 SC vehicle *ICV* versus E2 SC AICAR ICV; ###p < 0.001 versus sham or E2 SC vehicle ICV versus E2 SC AICAR ICV.

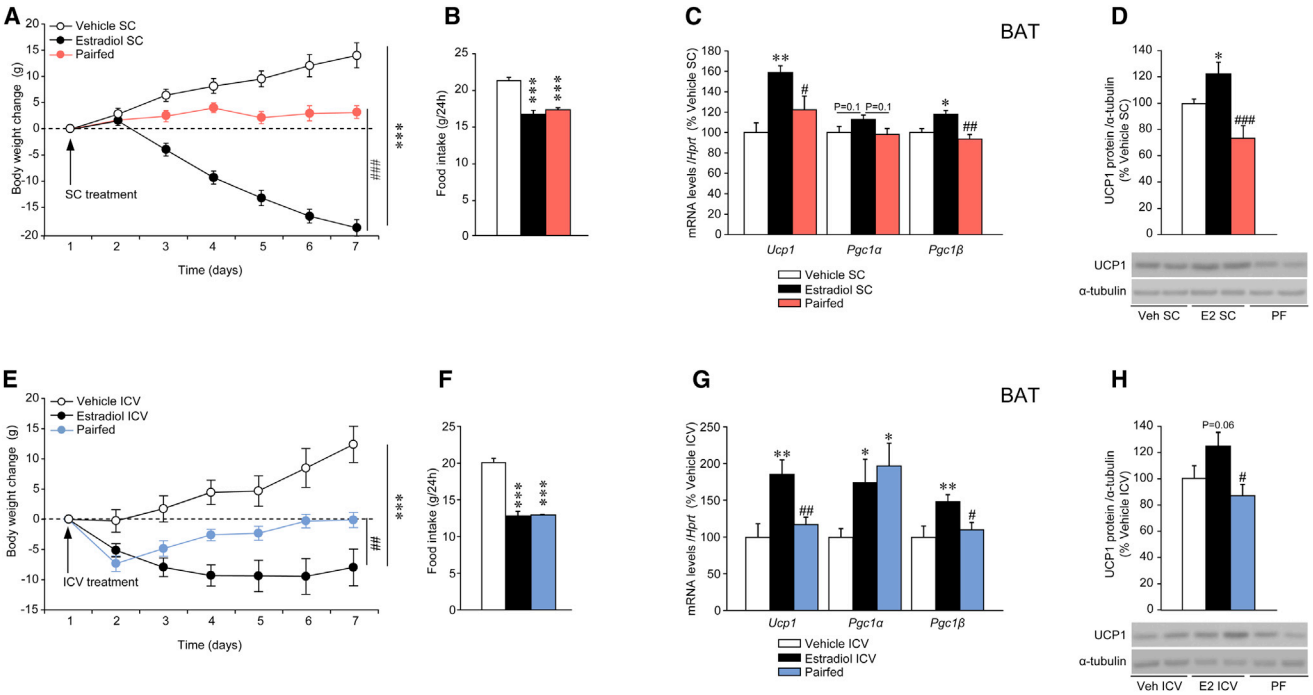


**Figure 2. Effect of SC and ICV E2 on BAT Thermogenic Markers**

(A–D) (A) Body weight change, (B) daily food intake, (C) mRNA expression profile in the BAT, and (D) protein levels (upper panel) and western blot autoradiographic images of BAT UCP1 protein (lower panel) of OVX rats treated with vehicle or E2 SC and pair-fed (PF) rats.

(E–H) (E) Body weight change, (F) daily food intake, (G) mRNA expression profile in the BAT, and (H) protein levels (upper panel) and western blot autoradiographic images of BAT UCP1 protein (lower panel) of OVX rats treated with vehicle or E2 ICV (5 nmol) and pair-fed rats. Error bars represent SEM; n = 8–20 animals per experimental group. *, **, and ***p < 0.05, 0.01, and 0.001 versus *v*ehicle (SC or ICV); #, ##, and ###p < 0.05, 0.01, and 0.001 versus E2 (SC or ICV).

in core temperature (Figure 4A). The increase in body temperature was associated with elevated UCP1 protein levels in BAT (Figure 4B) and a significant rise in the temperature of the skin surrounding interscapular BAT (Figure 4C), indicating elevated thermogenesis. No changes were detected in WAT browning program after ICV treatment with E2 (Figure S4A). The effects evoked by ICV E2 are not related to leakage of E2 from the cerebrospinal fluid, because circulating levels of E2 remain unchanged after ICV treatment (Figure S4B).

AMPK in VMH plays a major role in the modulation of BAT thermogenesis (López et al., 2010; Martínez de Morentin et al., 2012; Whittle et al., 2012). Thus, we aimed to investigate whether ICV E2 elicits changes in VMH AMPK signaling with ARC samples used as control. The specificity of the VMH and ARC dissections was confirmed by analyzing the mRNA of specific markers, namely SF1 and POMC, respectively (Figure S4C). We found that ICV administration of 1 nmol of E2 elicited similar changes to those observed in the MBH after 5 nmol of the hormone, namely decreased VMH AMPK activity (Figure 4D). ICV administration of 0.5 nmol of E2 also induced weight loss, anorexia, increased UCP1 in BAT, and decreased hypothalamic AMPK signaling (data not shown). No changes were found in the ARC AMPK pathway after ICV E2 injections (Figure S4D). Of note, the effect of ICV E2 administration was not related to increased inflammatory responses in the VMH (where, in fact, inflammatory markers showed reduced expression) (Figure S4E) or muscle (Figure S4F).

Given that ICV E2 induced a marked increase in the activity of the SNS subserving BAT, we aimed to investigate whether adrenergic receptors blockade impact the central effect of ICV E2 on BAT thermogenic program. Central administration of 1 nmol of E2 was reversed (in a feeding-independent manner) by pharmacological blockade of beta 3 adrenergic receptor (β3-AR) with the specific antagonist SR59230A (López et al., 2010) (Figures 4E and 4F). The increase in body weight induced by SR59230A was associated with appropriate reversal of ICV E2-induced activation of temperature (Figure 4G) and BAT UCP1 expression (Figure 4H).

## E2 within the VMH Regulates Hypothalamic AMPK and BAT Thermogenic Program

We performed stereotaxic administration of E2 into the VMH or the ARC. To assess the effects of E2 in both hypothalamic nuclei, we performed anatomical analysis of the injection routes, as well as a combined injection of vehicle or E2 with fluorescein-isothiocyanate (FITC), which allowed us to control the diffusion of the treatment. Both VMH and ARC injections were specific, and the treatment did not spread to other hypothalamic areas (Figure 5A); moreover, no damage in VMH or ARC structures was found when the sections were stained with toluidine blue (Figure S5A). We found that administration of E2 in the VMH, but not in the ARC, induced a significant rise in temperature (Figure 5B) associated with an upregulation of BAT UCP1 at both mRNA and protein levels (Figure 5C). In order to confirm these

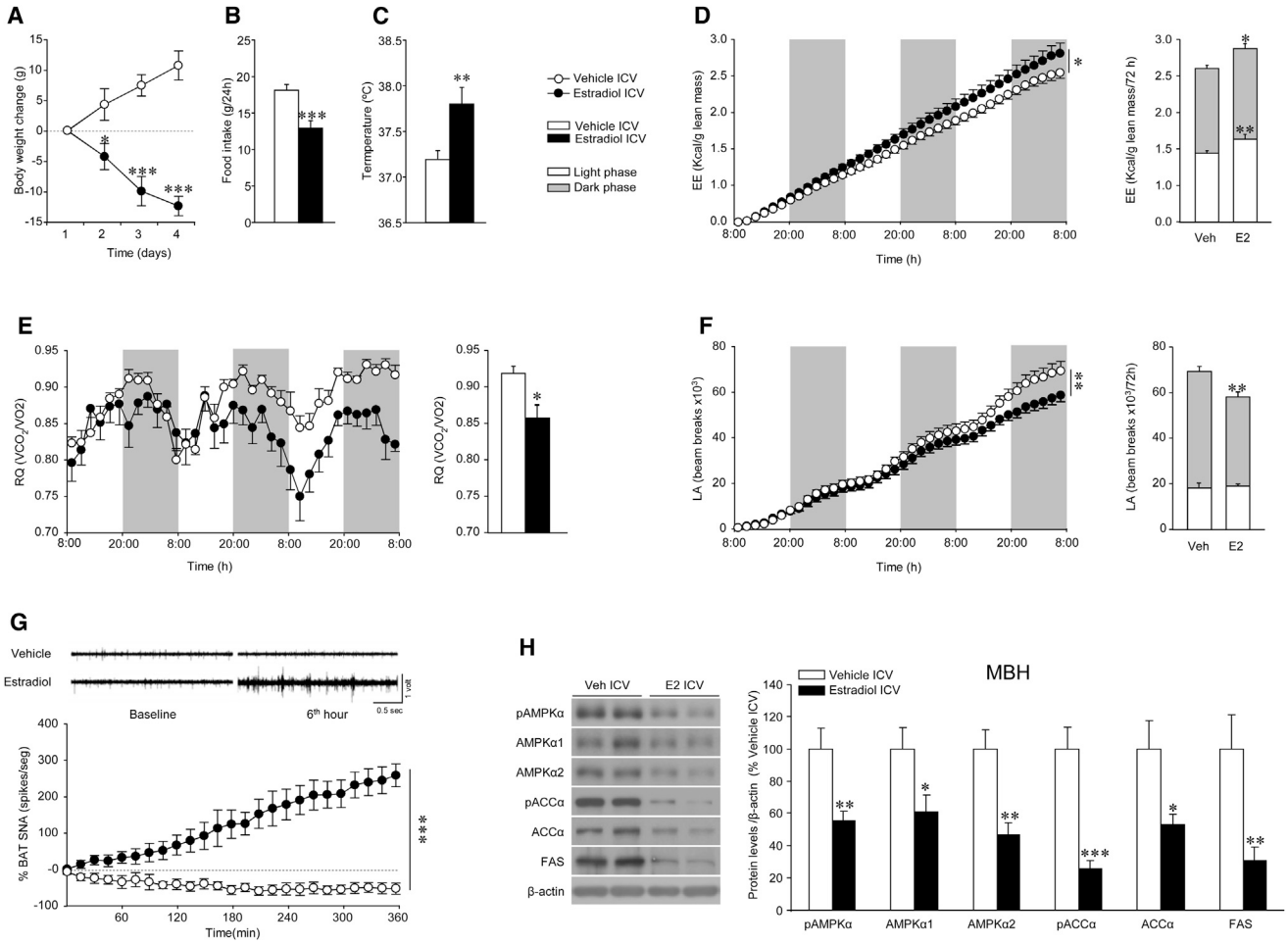


**Figure 3. Effect of ICV E2 on Energy Balance, BAT Activation, and Hypothalamic AMPK Pathway**

(A–H) (A) Body weight change, (B) daily food intake, (C) core temperature, (D) energy expenditure (EE) (cumulative in left panel and total in right panel), (E) respiratory quotient (RQ) (cumulative in left panel and total in right panel), (F) locomotor activity (LA) (cumulative in left panel and total in right panel), (G) BAT sympathetic nervous activity (SNA) tracings (upper panel) and time-course of BAT SNA response (lower panel), and (H) western blot autoradiographic images (left panel) and hypothalamic protein levels of proteins of the AMPK pathway (right panel) of OVX rats ICV treated with vehicle or E2 (5 nmol). Error bars represent SEM; n = 6 (SNA recordings) or 8–12 animals per experimental group. *, **, and ***p < 0.05, 0.01, and 0.001 *vs.* vehicle ICV.

data using an alternative approach, we used microdialysis, which recapitulated the E2-induced increase in BAT UCP1 (Figure S5C). To better control for the specificity of VMH administration, we performed "missed" E2 injections, in "VMH-neighboring" areas without affecting the VMH (Figure S5D). Our anatomical data showed that when VMH was not "hit" (as indicated by the absence of FITC in this nucleus), no changes in UCP1 expression in the BAT were detected (Figure S5E). This evidence indicates that the effect of E2 on BAT thermogenic program is specific of the VMH and it is not related to E2 spreading to adjacent areas. In line with the temperature and anatomical data, administration of E2 into the ARC did not affect the expression of thermogenic markers in the BAT (Figure 5D). In addition, these effects are not related to leakage or diffusion of central E2 from the brain, because circulating levels of E2 remained unchanged after VMH and ARC injections (Figure S5F).

We then assessed the effect of VMH and ARC E2 injection on the central mechanism modulating BAT thermogenic program. Rats receiving E2 in the VMH (but not ARC) displayed a significant increase in neuronal activation in the inferior olive (IO) and the raphe pallidus (RPa), as defined by c-FOS staining (Figure 5E). The RPa and IO have been involved in the sympathetic activation of BAT in response to cold (Shibata et al., 1999; Uno and Shibata, 2001; Cano et al., 2003; Cannon and Nedergaard, 2004). We also analyzed the effect of specific stereotaxic injection of E2 on the AMPK pathway in the VMH versus ARC. The administration of E2 into the VMH decreased the protein levels of pAMPK and pACC in this nucleus (Figure 5F; left images and graph). In contrast, no effect was detected on AMPK pathway when E2 was microinjected into the ARC (Figure 5F; right images and graph). AMPK is activated by phosphorylation of upstream kinases. The main upstream AMPK kinases are the tumor suppressor LKB1 and $Ca^{2+}$/calmodulin-dependent protein kinase kinase alpha and beta (CaMKKα and CaMKKβ), which phosphorylate AMPK at Thr172; AMPK phosphorylation levels are also regulated by protein phosphatase-2Cα (PP2Cα)

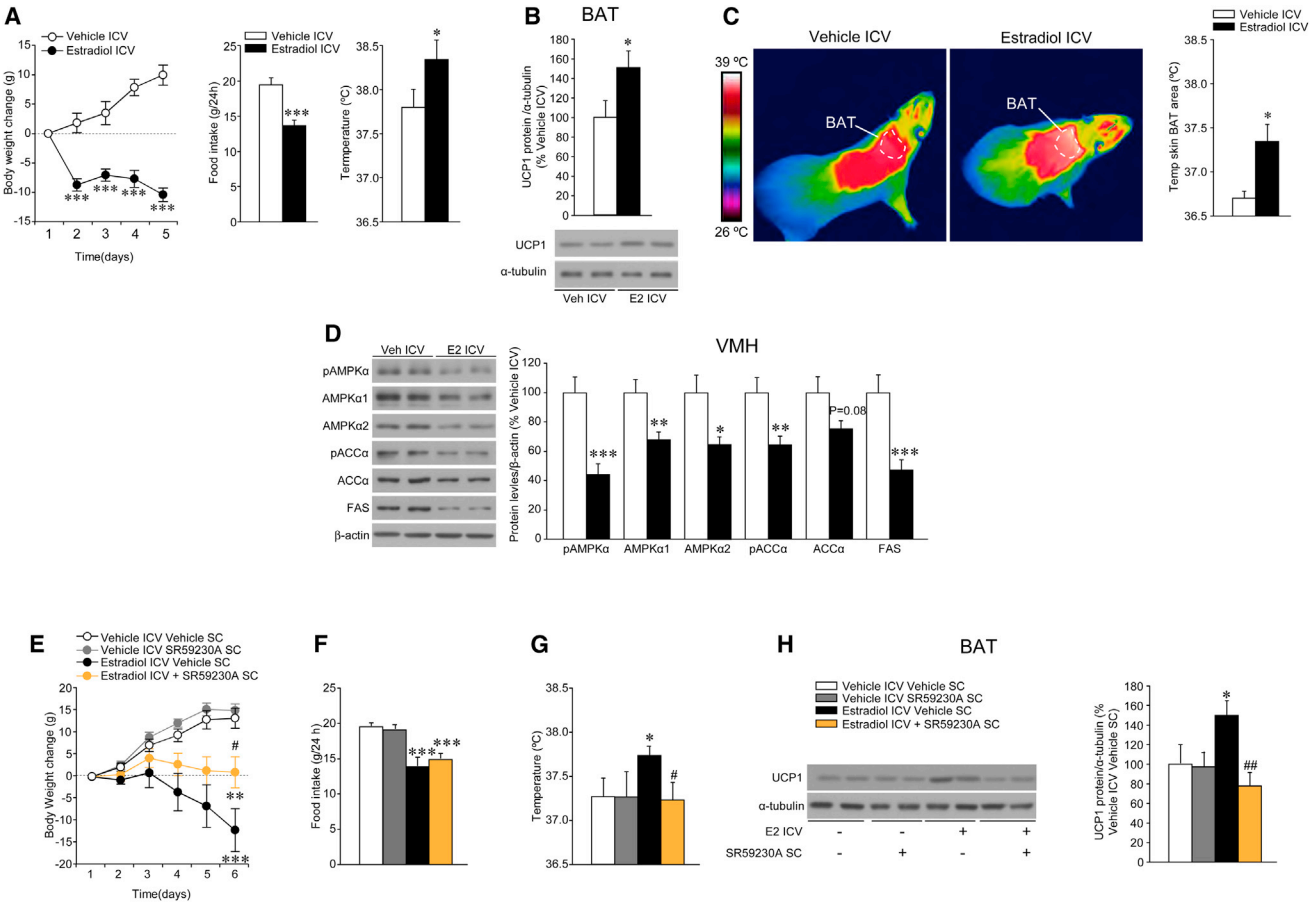


**Figure 4. Effect of ICV E2 on Energy Balance and the VMH AMPK-SNS-BAT Axis**

(A–D) (A) Body weight change (left panel), daily food intake (middle panel), and core temperature (right panel); (B) protein levels (upper panel) and western blot autoradiographic images of BAT UCP1 protein (lower panel); (C) infrared thermal images (left panel) and quantification of temperature of the skin surrounding interscapular BAT (right panel); and (D) western blot autoradiographic images (left panel) and VMH protein levels of proteins of the AMPK pathway (right panel) of OVX rats ICV treated with vehicle or E2 (1 nmol).

(E–H) (E) Body weight change, (F) daily food intake, (G) core temperature, and (H) western blot autoradiographic images of BAT UCP1 protein (left panel) and UCP1 protein levels (right panel) of OVX rats ICV treated with vehicle or E2 (1 nmol), previously SC treated with the β3-AR-antagonist SR59230A for 2 days. Error bars represent SEM; n = 7–12 animals per experimental group. * and ***p < 0.05 and 0.001 versus vehicle ICV or vehicle ICV vehicle SC; # and ##p < 0.05 and 0.01 versus E2 ICV vehicle SC.

(Carling et al., 2011; Hardie et al., 2012). We found that 2 hr after specific VMH E2 injection, the protein levels of CaMKKα and pLKB1 were decreased, whereas the levels of PP2Cα were increased in the VMH (Figure 5G). Consistent with these data, AMPK phosphorylation status was also reduced 2 hr after E2 treatment in the VMH (Figure S5G). Finally, E2 caused no changes in the activity of PI3K and AKT signaling in the VMH (just an increase in total AKT levels; Figure 5H), and as previously described (Gao et al., 2007), E2 induced a marked increase in the pSTAT3 levels in the VMH (Figure 5H).

## Activation of AMPK in the VMH Reverses the Central Action of E2

To elucidate the contribution of AMPK activity in the VMH to the thermogenic program in the BAT after E2 central treatment, adenoviruses encoding constitutively active AMPKα-CA, together with GFP or control adenovirus expressing GFP alone (Minokoshi et al., 2004; López et al., 2008, 2010; Martínez de Morentin et al., 2012; Whittle et al., 2012), were injected stereotaxically into the VMH or the ARC of OVX rats treated with vehicle or E2. Infection efficiency was assessed by (a) expression of GFP in the VMH (Figure 6A) or in the ARC (Figure 6E) and (b) increased phosphorylation of ACCα (Figure S6A). Quantification analyses showed that when the injections were directed to the VMH, the vast majority of GFP-positive cells (98.4%) reside in the VMH (Figure S6B). On the other hand, when the ARC was targeted, we achieved a similar level of specificity with 95% of GFP-positive cells in this nucleus (Figure S6C). Administration of AMPKα-CA adenoviruses into the VMH reversed the weight loss in OVX rats treated with E2 (Figure 6B) with no alteration in food intake (Figure 6C). Overexpression of AMPKα-CA in the VMH was also associated with a reduction in expression of UCP1, PGC1α, and PGC1β in the BAT, as well as reduced core temperature, of OVX rats treated with E2 (Figure 6D). This effect was VMH specific, since AMPKα-CA adenoviruses injected into the ARC of OVX rats treated with E2 caused a slight

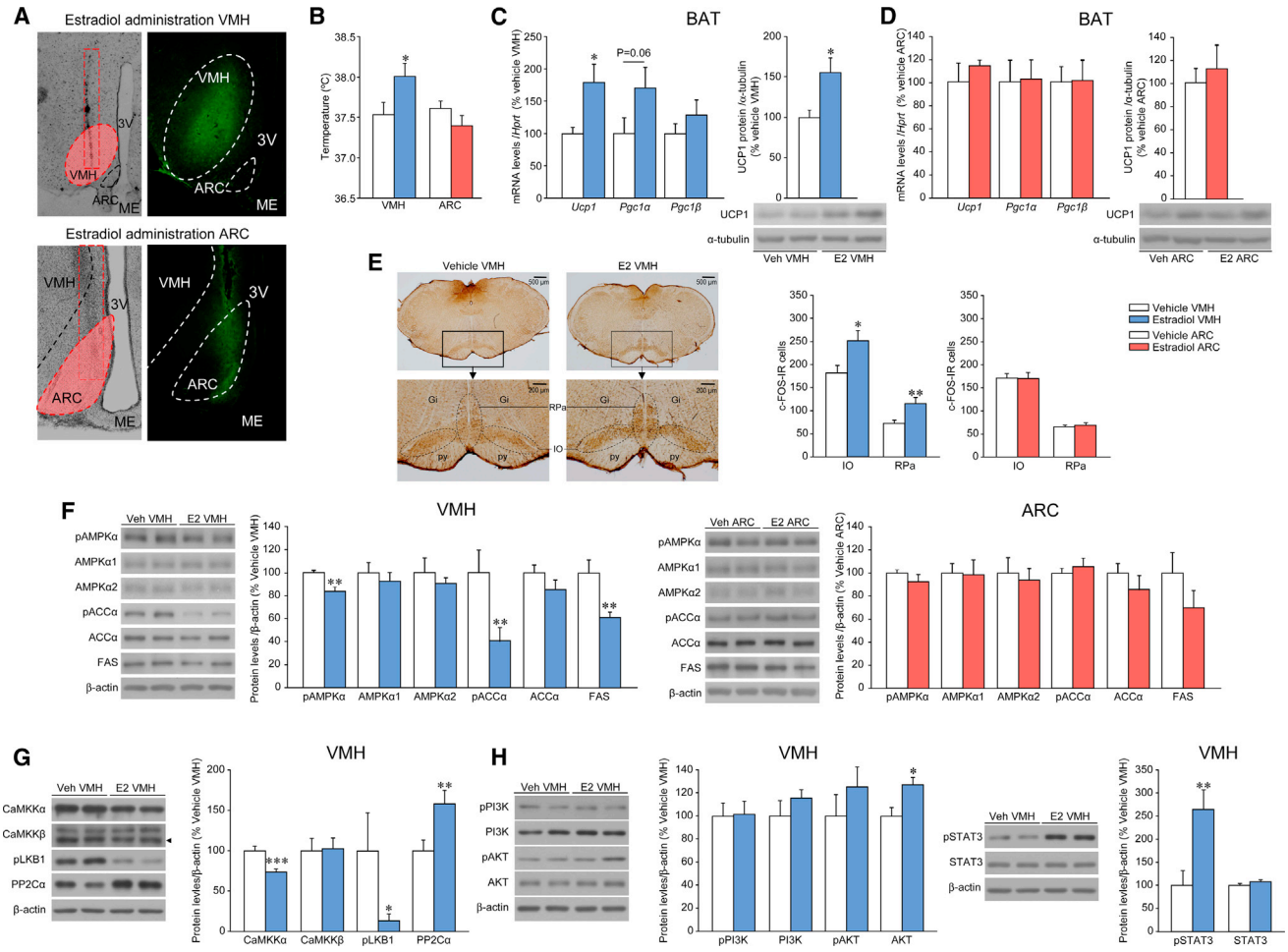


**Figure 5. Effect of E2 within the VMH or ARC on BAT Thermogenic Markers, Central SNS Outflow, and Hypothalamic AMPK Pathway**

(A) Representative photomicrographs of brain sections showing the injection route enclosed in a red rectangle, precisely placed in the VMH or ARC (10×, left panel), and immunofluorescence of brain sections (20×) showing the presence of the dye (FITC) after comicroinjection with E2 within the VMH or the ARC.

(B and C) (B) Core temperature and (C) mRNA expression profile in the BAT (left panel), protein levels (right-upper panel), and western blot autoradiographic images of BAT UCP1 (right-lower panel) of OVX rats stereotaxically treated with vehicle or E2 within the VMH.

(D) mRNA expression profile in the BAT (left panel), protein levels (right-upper panel), and western blot autoradiographic images of BAT UCP1 (right-lower panel) of rats stereotaxically treated with vehicle or E2 within the ARC.

(E) Representative photomicrographs (upper: 1.25×, lower 10×) showing immunohistochemistry of c-FOS (left panel) and c-FOS immunoreactive (IR) (right panel) cells in the inferior olive (IO) and the raphe pallidus (RPa) nuclei of OVX rats stereotaxically treated with vehicle or E2 within the VMH or ARC.

(F) Western blot autoradiographic images (left panels) and levels of proteins of the AMPK pathway (right panels) in the VMH or ARC of OVX rats stereotaxically treated with vehicle or E2 within the VMH (left images and graph) and the ARC (right images and graph); thus, when injection of E2 was performed in the VMH, the AMPK pathway was analyzed in the VMH, and when injection of E2 was performed in the ARC, the AMPK pathway was analyzed in the ARC.

(G and H) Western blot autoradiographic images (left panels) and protein levels (right panels) of (G) upstream kinases of AMPK and (H) PI3K/AKT pathway (left images and graph) and pSTAT3/STAT (right images and graph) in the VMH of OVX rats stereotaxically treated with vehicle or E2 within the VMH. Error bars represent SEM; n = 5 (c-FOS analysis) or 7–8 animals per experimental group. Gi: gigantocellular reticular nucleus; IO: inferior olive; ME: median eminence; py: pyramidal tract; RPa: raphe pallidus nucleus. *, ** and ***$p < 0.05$, 0.01, and 0.001 *vs.* vehicle VMH. In (A), it is important to note that the figure oversimplifies the protocol, since injections were given bilaterally.

increase in body weight in comparison to E2 GFP-treated rats (Figure 6F), which was associated with increased feeding (Figure 6G) but unaltered expression of thermogenic markers in the BAT (Figure 6H).

A particular feature of adenoviral experiments is that administration of AMPKα-CA had no effect on body weight per se in OVX animals treated with vehicle. A possible explanation for this is that AMPK was already maximally activated in the OVX state (data not shown). Thus, we determined whether chronic inactivation of AMPK in the VMH or the ARC can alter markers of BAT activation of OVX rats. Stereotaxic delivery of a dominant-negative isoform of AMPKα (AMPKα-DN) (Figure S6A) into the VMH, but not into the ARC, caused feeding-independent weight loss that began on the day following the injection (Figures S6D, S6E, S6G and S6H). Administration of AMPKα-DN into the VMH, but not into the ARC, of OVX rats increased the expression of UCP-1, PGC1α, and PGC1β in the BAT (Figures S6F and S6I).

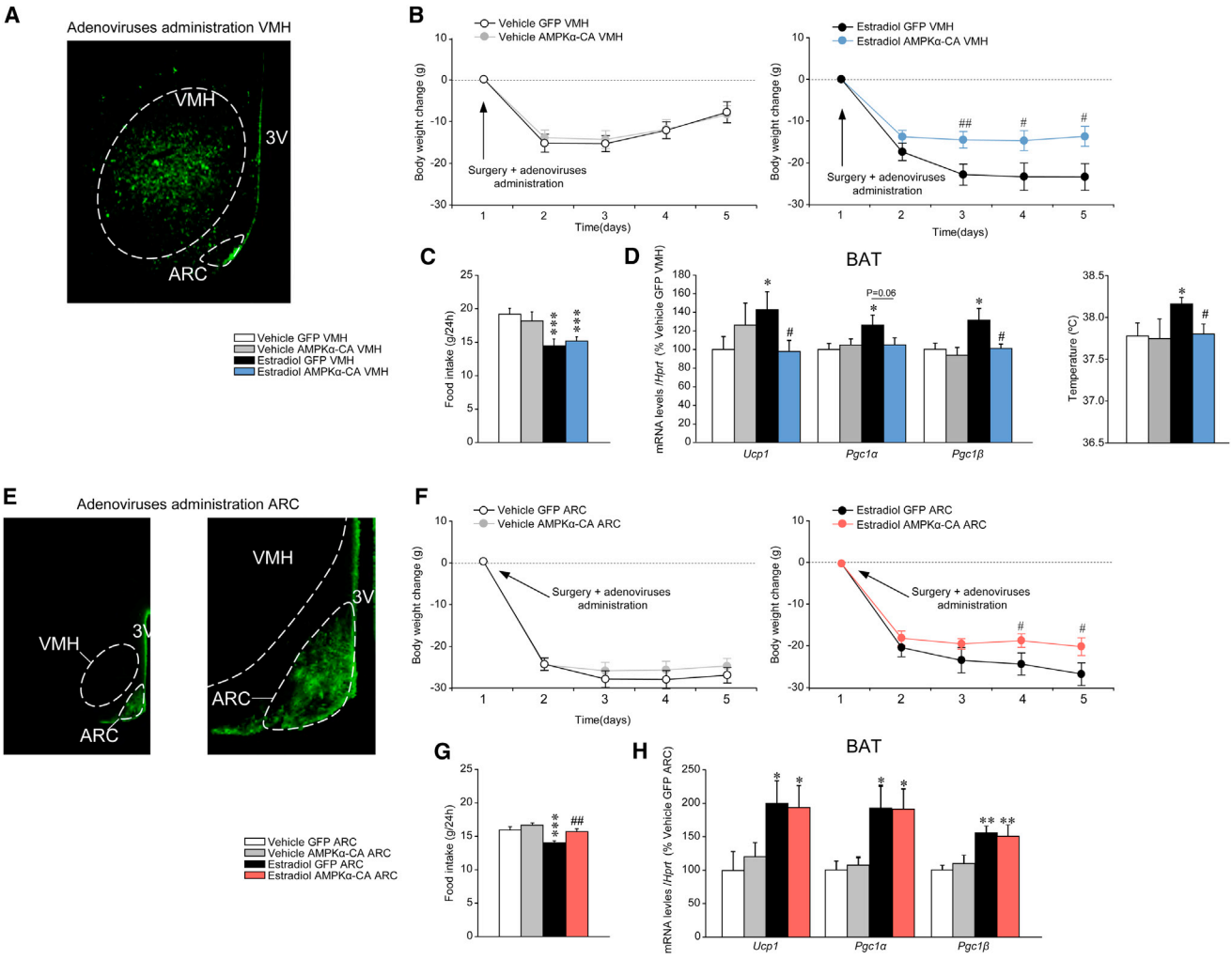


**Figure 6. Effect of Activation of Hypothalamic AMPK on the Central Actions of E2 on Energy Balance**

(A) Representative immunofluorescence (20×) with anti-GFP antibody showing GFP expression in the VMH of OVX rats treated with adenoviruses encoding AMPKα-CA within the VMH.

(B–D) (B) Body weight change, (C) daily food intake, and (D) mRNA expression profile in the BAT (left panel) and core temperature (at 24 hr, right panel) of OVX rats SC treated with vehicle or E2 (VMH in [D], right) and stereotaxically treated with GFP or AMPKα-CA adenoviruses within the VMH.

(E) Representative immunofluorescence (20×, left panel, and 40×, right panel) with anti-GFP antibody showing GFP expression in the ARC of rats treated with adenoviruses encoding AMPKα-CA within the ARC.

(F–H) (F) Body weight change, (G) daily food intake, and (H) mRNA expression profile in the BAT of OVX rats SC treated with vehicle or E2 and stereotaxically treated with GFP or AMPKα-CA adenoviruses within the ARC. Error bars represent SEM; n = 8–17 animals per experimental group. 3V: third ventricle; *, **, and ***p < 0.05 and 0.01 *vs.* vehicle GFP VMH or ARC; #, ## and ### p < 0.05 and 0.01versus E2 GFP VMH or ARC.

## The Physiological Actions of VMH E2 Are Mediated through ERα

To gain further insight into the physiological effects of endogenous E2 on the aforementioned VMH AMPK-SNS-BAT axis, we studied female rats at diestrus that display low-to-mid circulating levels of E2, in contrast to preovulatory animals with peak E2 concentrations (Figures S1B and 7A). Diestrus rats had higher core temperature (Figure 7A) and BAT UCP1 protein levels (Figure 7B) than OVX rats, as well as decreased AMPK signaling in the VMH (Figure 7C). Consistent with these data, ICV administration of the combined ERα-β antagonist ICI 182.780 (Movérare-Skrtic et al., 2014) to intact female rats induced feeding-independent weight gain (Figure S7A) in association with decreased UCP1 expression in the BAT (Figure S7B) and increased AMPK signaling in the VMH (Figure S7C).

ICV injections of the specific ERα antagonist MPP (Sun et al., 2002) to intact female rats induced weight gain and a tendency for food intake to increase (Figure 7D) in association with decreased BAT UCP1 expression (Figure 7E) and increased AMPK signaling in the VMH (Figure 7F). In keeping with this, ICV administration of the specific ERα agonist PPT (Sánchez-Criado et al., 2004, 2006; Roa et al., 2008) to OVX rats recapitulated the effects of E2 by eliciting weight loss and anorexia (Figure S7D), associated with increased UCP1 expression in BAT (Figure S7E) and reduced AMPK signaling in the VMH (Figure 7F). VMH administration of a lentivirus encoding an shRNA

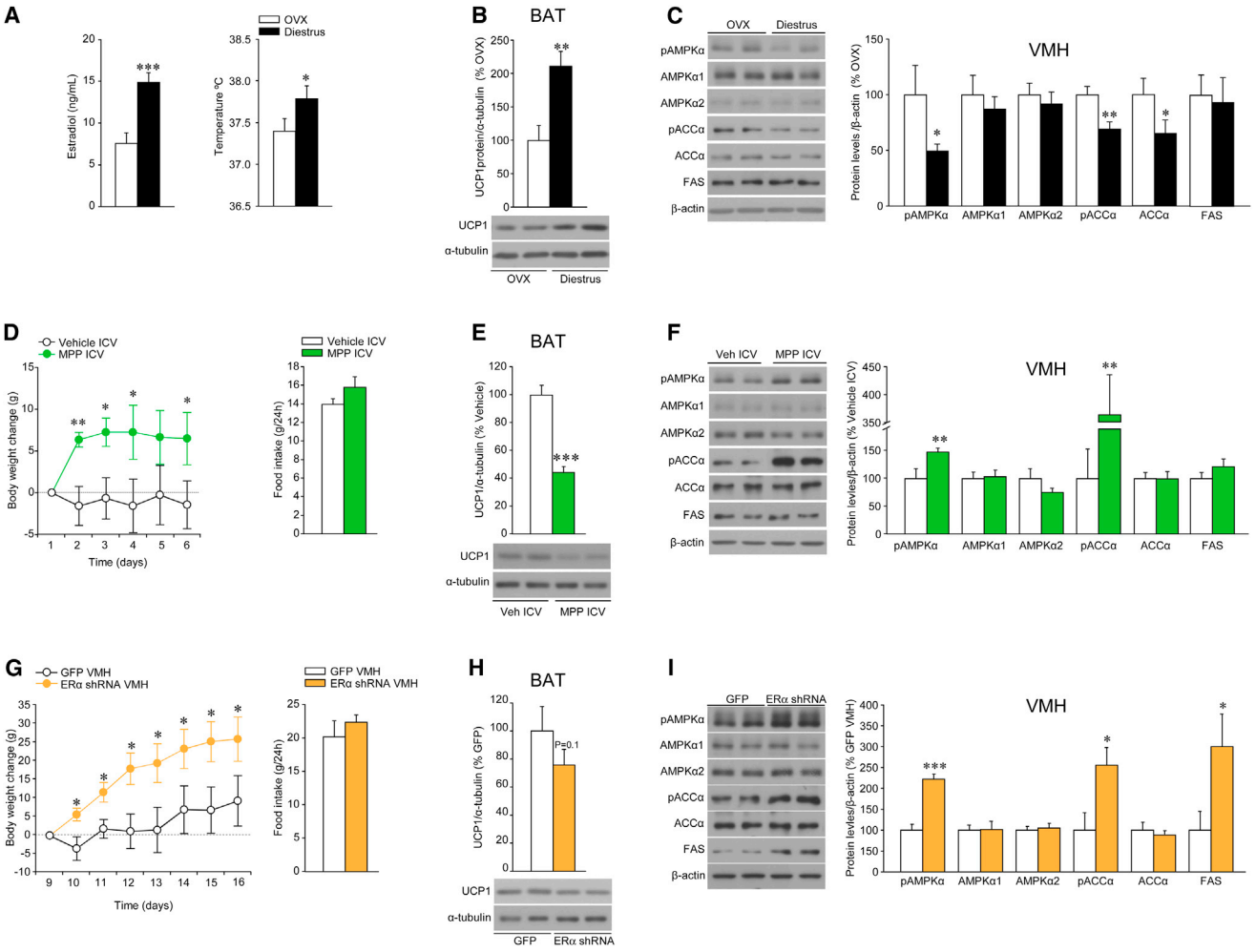


**Figure 7. Effect of Physiological Levels of E2 and Pharmacological and Genetic Manipulation of ERα on the VMH AMPK-SNS-BAT Axis**

(A–C) (A) Serum E2 levels (left panel) and core temperature (right panel), (B) protein levels (upper panel) and western blot autoradiographic images of BAT UCP1 protein (lower panel), and (C) western blot autoradiographic images (left panel) and levels of proteins of AMPK pathway in the VMH (right panel) of diestrus cycled rats. (D–F) (D) Body weight change (left panel) and daily food intake (right panel), (E) protein levels (upper panel) and western blot autoradiographic images of BAT UCP1 protein (lower panel), and (F) western blot autoradiographic images (left panel) and levels of proteins of AMPK pathway in the VMH (right panel) of intact rats ICV treated with the specific ERα antagonist MPP.

(G–I) (G) Body weight change (left panel) and daily food intake (right panel), (H) protein levels (upper panel) and western blot autoradiographic images of BAT UCP1 protein (lower panel), and (I) western blot autoradiographic images (left panel) and levels of proteins of AMPK pathway in the VMH (right panel) of intact rats stereotaxically treated within the VMH with lentivirus encoding short hairpin RNA of the ERα. Error bars represent SEM; n = 7–8 animals per experimental group. *, **, and ***p < 0.05, 0.01, and 0.001 versus OVX, vehicle ICV, or GFP VMH.

that silence ERα to intact female rats induced weight gain without changes in feeding behavior (Figure 7G) and simultaneous decrease in UCP1 expression in BAT (Figure 7H) and an increase in AMPK signaling in the VMH (Figure 7I). Conversely, overexpression of a wild-type isoform of ERα in the VMH of OVX rats, using adenoviral vector, induced feeding-independent weight loss (Figure S7G) in association with increased BAT UCP1 expression (Figure S7H) and decreased AMPK signaling in the VMH (Figure S7I).

## DISCUSSION

This study identifies a link between the effects of E2 on hypothalamic AMPK and BAT thermogenesis. Specifically, we show that activation of BAT thermogenic program and subsequent energy expenditure depends on ERα-mediated inactivation of VMH AMPK. Overall, these results offer a physiological mechanism, via the energy sensor AMPK, for the central actions of E2 on ERα that is of relevance in linking the changes in energy balance and obesity-associated alterations in the gonadal axis.

Conditions in which ovarian estrogens are lacking, such as OVX or menopause, are associated with hyperphagia and decreased caloric expenditure that results in a positive energy balance leading to obesity. Estrogen replacement reverts this phenotype both in women and female rodents (Carr, 2003; Gao and Horvath, 2008; Rogers et al., 2009; Wren, 2009; Finan et al., 2012; Mauvais-Jarvis et al., 2013). Recent evidence indicates that hypothalamic kisspeptin/neurokinin B/dynorphin

neurons promote cutaneous vasodilatation and participate in the E2 modulation of body temperature (Mittelman-Smith et al., 2012; Rance et al., 2013). Also, genetic models have shown that some of the actions of estrogens on energy homeostasis are centrally mediated through activation of ERα in key hypothalamic nuclei, such as the ARC and the VMH (Musatov et al., 2007; Xu et al., 2011). In this regard, compelling data have demonstrated that E2, the most important ovarian estrogen, inhibits feeding in a leptin-independent (but STAT3-dependent) manner, acting on POMC, NPY, and melanin-concentrating hormone (MCH) neurons in the hypothalamus (Mystkowski et al., 2000; Gao et al., 2007). Furthermore, it has been proposed that E2 modulates ghrelin signaling and that this endocrine interaction may account for important sex differences in the regulation of food intake (Clegg et al., 2007). However, E2 action on feeding does not explain the entire change in body weight, as shown here in experiments assessing the effect of estrogens in pair-fed animals.

Recent literature indicates that hypothalamic AMPK pathway is a central regulator of energy homeostasis that acts by controlling both feeding and energy dissipation (Minokoshi et al., 2004; López et al., 2008, 2010; Andrews et al., 2008; Martínez de Morentin et al., 2012; Whittle et al., 2012). Therefore, we hypothesized that E2-induced actions on energy balance could be mediated by hypothalamic AMPK. Our data showed that peripheral administration of E2 induced a negative energy balance in obese and hyperphagic OVX rats, associated with inactivation of AMPK signaling and increased malonyl-CoA levels in the hypothalamus. Notably, central pharmacological activation of AMPK, using AICAR, was able to restore hypothalamic malonyl-CoA concentration and reversed the anorectic effect evoked by E2 administration. Overall, these data indicate that hypothalamic AMPK mediated the actions of E2 on energy balance. These results are in line with previous evidence suggesting an anabolic role for AMPK in the hypothalamus, which is in contrast with its peripheral catabolic function (Minokoshi et al., 2002; Minokoshi et al., 2004; Narkar et al., 2008). Of note, the effects of peripherally administered E2 were recapitulated by its central injection. ICV administration of E2 promoted a state of negative energy balance, characterized by hypophagia, increased energy expenditure, and BAT thermogenesis, leading to marked weight loss. This effect was associated with a robust decrease in hypothalamic AMPK signaling, neuronal activation in RPa and IO (two nuclei which have been functionally linked to the regulation of BAT thermogenesis) (Morrison, 1999; Shibata et al., 1999; Uno and Shibata, 2001; Cano et al., 2003; Morrison et al., 2014), and increased SNS tone to BAT. While based on the literature we do believe that our activation (c-FOS) data in IO and caudal RPa are related to BAT activity, we cannot rule out the possibility that at least part of the responses observed might be related to other functions, such as motor control, as previously described (Welsh and Llinás, 1997; Apps, 1999). Importantly, the above effects are reversed by pharmacological blockage of β3-AR and appear to derive from VMH-specific actions of E2, so that the impact of E2 on BAT thermogenesis derives from its ability to modulate AMPK activity in the VMH. Interestingly, when E2 was given in the neighboring ARC, which has been primarily involved in the regulation of feeding rather than energy expenditure (Williams and Elmquist, 2012; Yeo and Heisler, 2012), no effect was detected on BAT thermogenic program. Likewise, genetic activation of AMPK within the VMH, but not in the ARC, abolished the effect of central E2 on BAT program markers. In contrast, genetic activation of AMPK in the ARC reversed E2 anorectic action but had no effects on BAT function.

Overall, these data confirm that E2 modulates energy homeostasis in a brain site-specific fashion (Xu et al., 2011) and uncover a molecular mechanism (i.e. modulation of AMPK, by which E2 specifically modulates BAT metabolism). Also, in agreement with elegant studies from Clegg and colleagues (Heine et al., 2000; Musatov et al., 2007; Xu et al., 2011), our data using pharmacological and viral approaches also suggest that the effect of E2 on the VMH AMPK-SNS-BAT axis is mediated by ERα. Remarkably, physiological fluctuations in E2 levels during estrous cycle and blockade of E2 actions also modulate the aforementioned axis, indicating that this integrative response is not a particular phenomenon restricted to conditions of estrogen deficiency, such as OVX, but also a mechanism of relevance in the physiological regulation of energy homeostasis by ovarian estrogens.

In recent years, hypothalamic metabolic energy sensors, such as AMPK, have been suggested to play a major role in the regulation of energy homeostasis. Several metabolic hormones, such as leptin, ghrelin, insulin, and thyroid hormones (Minokoshi et al., 2004; Andrews et al., 2008; López et al., 2008, 2010), and more recently bone morphogenetic protein 8b (BMP8b) (Whittle et al., 2012), have been shown to regulate energy balance acting through those energy sensors. Here, we provide evidence that E2, a hormone that markedly influences energy and metabolic homeostasis, acts on the same sensors to control both feeding and energy expenditure. Notably, the mechanisms described here for the thermogenic actions of E2 display considerable commonalities with those previously unveiled by our group for thyroid hormone and BMP8b (López et al., 2010; Whittle et al., 2012). Thus, the VMH AMPK-SNS-BAT axis appears to act as a canonical central mechanism integrating central and peripheral regulation of energy stores. In this regard, our data points to AMPK in the VMH as a potential target for the treatment of obesity and other metabolic disorders associated to conditions of endocrine deregulation. The relevance of such a pharmacological target is emphasized by recent reports showing that nicotine-induced anorexia and weight loss is in part mediated by actions on AMPK-expressing neurons in the VMH to increase energy expenditure (Martínez de Morentin et al., 2012), which could be exploited as a potential therapeutic strategy. In addition, DiMarchi, Tschop, and colleagues have recently reported an elegant approach based on the development of a combinatorial peptide of a glucagon-like peptide-1 (GLP-1)-estrogen conjugate for the treatment of obesity and metabolic syndrome (Finan et al., 2012). They demonstrated that selective activation of ERs in GLP-1-targeted tissues enhances the benefits of both E2 and GLP-1 agonism on body weight, glucose homeostasis, and lipid metabolism. Considering that both GLP-1 receptor and ERα are highly expressed in the VMH (Shughrue et al., 1997; Gu et al., 2013) raises the possibility that the metabolic benefits of E2 and GLP-1 agonism may be mediated by selective modulation of AMPK in the VMH. However, further investigations are needed to test such possibility.

In summary, we show that central E2 inactivates AMPK in the VMH through ERα, which increases SNS tone, upregulates BAT thermogenesis, and increases energy expenditure, leading to weight loss. Thus, our data add more evidence to the fact that AMPK, specifically in the VMH, is a canonical mechanism modulating energy dissipation via SNS activation of BAT. This observation provides insights into the physiological regulation of energy balance and its perturbation in estrogen-deficient states and suggests that the VMH AMPK-SNS-BAT axis may be a potential therapeutic target for the treatment of obesity.

## EXPERIMENTAL PROCEDURES

### Animals

Female Sprague-Dawley and Wistar Unilever (for the microdialysis experiments) rats (250–300 g; Animalario General USC, Santiago de Compostela, Spain; Harlan, Horst, The Netherlands; and Charles River, Wilmington) were used for the experiments. All animals were housed on a 12 hr light (8:00 to 20:00) 12 hr dark cycle, in a temperature- and humidity-controlled room. The animals were allowed free access to standard laboratory pellets of rat chow and tap water. The experiments were performed in agreement with the International Law on Animal Experimentation and were approved by the USC Local Ethical Committee and the Ministry of Science and Innovation of Spain (Project ID PI12/01814), Animal Experimental Committee of the AMC, and the University of Iowa Institutional Animal Care and Use Committee.

### OVX

Sprague-Dawley rats were bilaterally ovariectomized (OVX) or sham operated, as described previously, under ketamine/xylacine anesthesia (50 mg/kg, intraperitoneally) (Vigo et al., 2007; Roa et al., 2009; Liu et al., 2013). All treatments (central or peripheral) on OVX rats were carried out 2 weeks after surgery to ensure a total washout of endogenous ovarian hormones. For the experiments of E2 replacement, OVX rats received a daily SC injection of E2 (estradiol benzoate; EB, 2 μg dissolved in 100 μL of sesame oil; both from Sigma; Saint Louis) or vehicle (100 μL of sesame oil; control rats) during 7 days. EB was chosen for SC administration, as this synthetic estrogen is endowed with higher bio-potency and stability and it has been often used in various protocols of peripheral estrogenization (Clegg et al., 2007; Roa et al., 2008).

### Central and Peripheral Treatments

Chronic ICV cannulae were implanted as described previously (see Supplemental Experimental Procedures). We used 17β-estradiol (17β-E2, as the major endogenous estrogen) in our central (ICV, VMH, or ARC) experiments in a mix DMSO:saline (1:10). Intact female (see below) or OVX rats were subjected to a protocol of daily ICV injections of *17β-E2* (0.5 nmol, 1 nmol, or 5 nmol dissolved in 5 μl of saline containing 10% of DMSO; Sigma; Saint Louis) or vehicle (5 μl of saline containing 10% of DMSO; control rats) for 3–7 days. For the experiments of pharmacological AMPK activation, rats were ICV treated with AICAR (5 μg dissolved in 5 μl of DMSO; Sigma, Saint Louis) or vehicle (5 μl of DMSO), for 2 and 4 hr. For the experiments of ER stimulation of blockage, we used ICV administration of the following: (a) the selective estrogen receptor alpha (ERα) agonist PPT (1 nmol dissolved in 5 μL of saline containing 10% of DMSO; TOCRIS Bioscience, Bristol) (Roa et al., 2008), (b) the combined ERα-β antagonist named ICI 182.780 (2.5 nmol dissolved in 5 μl of saline containing 10% of DMSO; TOCRIS Bioscience, Bristol) (Movérare-Skrtic et al., 2014), (c) and the specific ERα antagonist MPP (2.5 nmol dissolved in 5 μl of saline containing 10% of DMSO; TOCRIS Bioscience, Bristol) (Harrington et al., 2003). Both ICI 182.780 and MPP were administrated to intact female rats. The β3-AR specific antagonist SR59230A (3 mg/kg/day; Tocris Bioscience, Bristol) (López et al., 2010) was administrated subcutaneously, starting during 2 days before the ICV E2 injections. For more details of implantation of microdialysis probes and central treatments, see Supplemental Experimental Procedures.

### Stereotaxic Treatments of E2 and Viral Vectors

Freely moving rats were treated within the VMH or ARC with 17β-E2 (Sigma, Saint Louis; 0.1 nmol in 1 μl of saline containing 10% of DMSO) or vehicle (1 μl of saline containing 10% of DMSO) during 2 or 12 hr. FITC (Sigma, Saint Louis) was used to control the diffusion of the treatment. Adenoviral (GFP, AMPKα-CA, or AMPKα-DN: Viraquest, North Liberty; ERα wildtype: Signagen; Rockville) or lentiviral (GFP, ERα shRNA; Santa Cruz Biotechnology; Santa Cruz) were stereotaxically delivered as previously reported (López et al., 2008, 2010; Martínez de Morentin et al., 2012; Whittle et al., 2012; Schneeberger et al., 2013). Animals were treated for 5–7 days in the case of adenoviruses and 16 days in the case of lentiviruses, due to the longer infective period needed.

### Sample Processing and Analytical Methods

Sample processing, analysis of EE, LA, and RQ; nuclear magnetic resonance analysis; sympathetic nerve activity (SNA) recording; temperature measurements; E2, LH, and malonyl-CoA assays; and real-time quantitative PCR, in situ hybridization, western blotting, and immunohistochemistry were performed as previously shown (López et al., 2008, 2010; Martínez de Morentin et al., 2012; Whittle et al., 2012; Schneeberger et al., 2013) (see Supplemental Experimental Procedures for detailed protocols).

### Statistical Analysis

Data are expressed as mean ±SEM. mRNA and protein data were expressed in relation (%) to control (vehicle-treated) rats. Error bars represent SEM. Statistical significance was determined by Student's t test when two groups were compared or ANOVA and post hoc two-tailed Bonferroni test when more than two groups were compared. $p < 0.05$ was considered significant.

## SUPPLEMENTAL INFORMATION

Supplemental Information includes seven figures, one table, and Supplemental Experimental Procedures and can be found with this article online at http://dx.doi.org/10.1016/j.cmet.2014.03.031.

## AUTHOR CONTRIBUTIONS

P.B.M.M., I.G.-G., L.M., R.L., D.F.-M., N.M.-S., F.R.-P., and L.P. performed the in vivo experiments (hormonal, drug, and viral treatments), the analytical methods (in situ hybridization, western blotting, real-time quantitative PCR, and hormone measurements), the analysis of temperature, EE, RQ, LA, and NMR. They also analyzed and collected the data. J.L., A.K., E.F., and P.H.B. performed the microdialysis experiments. D.A.M. and K.R. performed the SNA recording. R.G. performed the immunohistochemistry. A.K.S. performed the malonyl-CoA analysis. P.B.M.M., A.K., E.F., C.D., R.N., K.R., M.T.-S., and M.L. designed the experiments and analyzed, discussed, and interpreted the data; P.B.M.M., A.K., E.F., C.D., R.N., K.R., M.T.-S., and M.L. reviewed and edited the manuscript; P.B.M.M. and M.L. made the figures. M.L. developed the hypothesis, coordinated and directed the project, and wrote the manuscript. All authors had final approval of the submitted manuscript.

## ACKNOWLEDGEMENTS

The research leading to these results has received funding from the European Community's Seventh Framework Programme (FP7/2007-2013) under grant agreement n° 281854, the ObERStress European Research Council Project (M.L.), and 245009, the Neurofast project (R.N., C.D., and M.L.); Xunta de Galicia (R.N.: EM 2012/039 and 2012-CP069; M.L.: 2012-CP070); Junta de Andalucía (M.T.S.: P08-CVI-03788); Instituto de Salud Carlos III (ISCIII) (M.L.: PI12/01814); MINECO cofunded by the FEDER Program of EU (M.T.S.: BFU2011-25021; R.N.: RyC-2008-02219 and BFU2012-35255; C.D.: BFU2011-29102); KNAW (P.H.B.: CEP-09CDP030); ZonMw (A.K.: TOP91207036); and NIH (K.R.: HL084207). L.M. is a recipient of a fellowship from Fundação para a Ciência e Tecnologia, Portugal (SFRH/BD/65379/2009). I.G.-G. is a recipient of a fellowship from Ministerio de Educación, Cultura y Deporte (FPU12/01827). CIBER de Fisiopatología de la Obesidad y Nutrición is an initiative of ISCIII.

Received: May 17, 2013
Revised: February 16, 2014
Accepted: March 26, 2014
Published: May 22, 2014

## REFERENCES

Andrews, Z.B., Liu, Z.W., Walllingford, N., Erion, D.M., Borok, E., Friedman, J.M., Tschöp, M.H., Shanabrough, M., Cline, G., Shulman, G.I., et al. (2008). UCP2 mediates ghrelin's action on NPY/AgRP neurons by lowering free radicals. Nature *454*, 846–851.

Apps, R. (1999). Movement-related gating of climbing fibre input to cerebellar cortical zones. Prog. Neurobiol. *57*, 537–562.

Cannon, B., and Nedergaard, J. (2004). Brown adipose tissue: function and physiological significance. Physiol. Rev. *84*, 277–359.

Cano, G., Passerin, A.M., Schiltz, J.C., Card, J.P., Morrison, S.F., and Sved, A.F. (2003). Anatomical substrates for the central control of sympathetic outflow to interscapular adipose tissue during cold exposure. J. Comp. Neurol. *460*, 303–326.

Carling, D., Mayer, F.V., Sanders, M.J., and Gamblin, S.J. (2011). AMP-activated protein kinase: nature's energy sensor. Nat. Chem. Biol. *7*, 512–518.

Carr, M.C. (2003). The emergence of the metabolic syndrome with menopause. J. Clin. Endocrinol. Metab. *88*, 2404–2411.

Clegg, D.J., Brown, L.M., Zigman, J.M., Kemp, C.J., Strader, A.D., Benoit, S.C., Woods, S.C., Mangiaracina, M., and Geary, N. (2007). Estradiol-dependent decrease in the orexigenic potency of ghrelin in female rats. Diabetes *56*, 1051–1058.

Finan, B., Yang, B., Ottaway, N., Stemmer, K., Müller, T.D., Yi, C.X., Habegger, K., Schriever, S.C., García-Cáceres, C., Kabra, D.G., et al. (2012). Targeted estrogen delivery reverses the metabolic syndrome. Nat. Med. *18*, 1847–1856.

Fisher, F.M., Kleiner, S., Douris, N., Fox, E.C., Mepani, R.J., Verdeguer, F., Wu, J., Kharitonenkov, A., Flier, J.S., Maratos-Flier, E., and Spiegelman, B.M. (2012). FGF21 regulates PGC-1α and browning of white adipose tissues in adaptive thermogenesis. Genes Dev. *26*, 271–281.

Gao, Q., and Horvath, T.L. (2008). Cross-talk between estrogen and leptin signaling in the hypothalamus. Am. J. Physiol. Endocrinol. Metab. *294*, E817–E826.

Gao, Q., Mezei, G., Nie, Y., Rao, Y., Choi, C.S., Bechmann, I., Leranth, C., Toran-Allerand, D., Priest, C.A., Roberts, J.L., et al. (2007). Anorectic estrogen mimics leptin's effect on the rewiring of melanocortin cells and Stat3 signaling in obese animals. Nat. Med. *13*, 89–94.

García, M.C., López, M., Gualillo, O., Seoane, L.M., Diéguez, C., and Señarís, R.M. (2003). Hypothalamic levels of NPY, MCH, and prepro-orexin mRNA during pregnancy and lactation in the rat: role of prolactin. FASEB J. *17*, 1392–1400.

Grumbach, M.M., and Auchus, R.J. (1999). Estrogen: consequences and implications of human mutations in synthesis and action. J. Clin. Endocrinol. Metab. *84*, 4677–4694.

Gu, G., Roland, B., Tomaselli, K., Dolman, C.S., Lowe, C., and Heilig, J.S. (2013). Glucagon-like peptide-1 in the rat brain: distribution of expression and functional implication. J. Comp. Neurol. *521*, 2235–2261.

Hardie, D.G., Ross, F.A., and Hawley, S.A. (2012). AMPK: a nutrient and energy sensor that maintains energy homeostasis. Nat. Rev. Mol. Cell Biol. *13*, 251–262.

Harrington, W.R., Sheng, S., Barnett, D.H., Petz, L.N., Katzenellenbogen, J.A., and Katzenellenbogen, B.S. (2003). Activities of estrogen receptor alpha- and beta-selective ligands at diverse estrogen responsive gene sites mediating transactivation or transrepression. Mol. Cell. Endocrinol. *206*, 13–22.

Heine, P.A., Taylor, J.A., Iwamoto, G.A., Lubahn, D.B., and Cooke, P.S. (2000). Increased adipose tissue in male and female estrogen receptor-alpha knockout mice. Proc. Natl. Acad. Sci. USA *97*, 12729–12734.

Hill, J.W., Alreja, M., and Elias, C.F. (2013). From precocious puberty to infertility: metabolic control of the reproductive function. Front. Endocrinol. (Lausanne) *4*, 43.

Jones, M.E., Thorburn, A.W., Britt, K.L., Hewitt, K.N., Wreford, N.G., Proietto, J., Oz, O.K., Leury, B.J., Robertson, K.M., Yao, S., and Simpson, E.R. (2000). Aromatase-deficient (ArKO) mice have a phenotype of increased adiposity. Proc. Natl. Acad. Sci. USA *97*, 12735–12740.

Jones, M.E., Thorburn, A.W., Britt, K.L., Hewitt, K.N., Misso, M.L., Wreford, N.G., Proietto, J., Oz, O.K., Leury, B.J., Robertson, K.M., et al. (2001). Aromatase-deficient (ArKO) mice accumulate excess adipose tissue. J. Steroid Biochem. Mol. Biol. *79*, 3–9.

Liu, J., Bisschop, P.H., Eggels, L., Foppen, E., Ackermans, M.T., Zhou, J.N., Fliers, E., and Kalsbeek, A. (2013). Intrahypothalamic estradiol regulates glucose metabolism via the sympathetic nervous system in female rats. Diabetes *62*, 435–443.

López, M., Lage, R., Saha, A.K., Pérez-Tilve, D., Vázquez, M.J., Varela, L., Sangiao-Alvarellos, S., Tovar, S., Raghay, K., Rodríguez-Cuenca, S., et al. (2008). Hypothalamic fatty acid metabolism mediates the orexigenic action of ghrelin. Cell Metab. *7*, 389–399.

López, M., Varela, L., Vázquez, M.J., Rodríguez-Cuenca, S., González, C.R., Velagapudi, V.R., Morgan, D.A., Schoenmakers, E., Agassandian, K., Lage, R., et al. (2010). Hypothalamic AMPK and fatty acid metabolism mediate thyroid regulation of energy balance. Nat. Med. *16*, 1001–1008.

Martínez de Morentin, P.B., Whittle, A.J., Fernø, J., Nogueiras, R., Diéguez, C., Vidal-Puig, A., and López, M. (2012). Nicotine induces negative energy balance through hypothalamic AMP-activated protein kinase. Diabetes *61*, 807–817.

Mauvais-Jarvis, F., Clegg, D.J., and Hevener, A.L. (2013). The role of estrogens in control of energy balance and glucose homeostasis. Endocr. Rev. *34*, 309–338.

Minokoshi, Y., Kim, Y.B., Peroni, O.D., Fryer, L.G., Müller, C., Carling, D., and Kahn, B.B. (2002). Leptin stimulates fatty-acid oxidation by activating AMP-activated protein kinase. Nature *415*, 339–343.

Minokoshi, Y., Alquier, T., Furukawa, N., Kim, Y.B., Lee, A., Xue, B., Mu, J., Foufelle, F., Ferré, P., Birnbaum, M.J., et al. (2004). AMP-kinase regulates food intake by responding to hormonal and nutrient signals in the hypothalamus. Nature *428*, 569–574.

Mittelman-Smith, M.A., Williams, H., Krajewski-Hall, S.J., McMullen, N.T., and Rance, N.E. (2012). Role for kisspeptin/neurokinin B/dynorphin (KNDy) neurons in cutaneous vasodilatation and the estrogen modulation of body temperature. Proc. Natl. Acad. Sci. USA *109*, 19846–19851.

Morrison, S.F. (1999). RVLM and raphe differentially regulate sympathetic outflows to splanchnic and brown adipose tissue. Am. J. Physiol. *276*, R962–R973.

Morrison, S.F., Madden, C.J., and Tupone, D. (2014). Central neural regulation of brown adipose tissue thermogenesis and energy expenditure. Cell Metab. http://dx.doi.org/10.1016/j.cmet.2014.02.007.

Movérare-Skrtic, S., Börjesson, A.E., Farman, H.H., Sjögren, K., Windahl, S.H., Lagerquist, M.K., Andersson, A., Stubelius, A., Carlsten, H., Gustafsson, J.A., and Ohlsson, C. (2014). The estrogen receptor antagonist ICI 182,780 can act both as an agonist and an inverse agonist when estrogen receptor α AF-2 is modified. Proc. Natl. Acad. Sci. USA *111*, 1180–1185.

Musatov, S., Chen, W., Pfaff, D.W., Mobbs, C.V., Yang, X.J., Clegg, D.J., Kaplitt, M.G., and Ogawa, S. (2007). Silencing of estrogen receptor alpha in the ventromedial nucleus of hypothalamus leads to metabolic syndrome. Proc. Natl. Acad. Sci. USA *104*, 2501–2506.

Mystkowski, P., Seeley, R.J., Hahn, T.M., Baskin, D.G., Havel, P.J., Matsumoto, A.M., Wilkinson, C.W., Peacock-Kinzig, K., Blake, K.A., and Schwartz, M.W. (2000). Hypothalamic melanin-concentrating hormone and estrogen-induced weight loss. J. Neurosci. *20*, 8637–8642.

Narkar, V.A., Downes, M., Yu, R.T., Embler, E., Wang, Y.X., Banayo, E., Mihaylova, M.M., Nelson, M.C., Zou, Y., Juguilon, H., et al. (2008). AMPK and PPARdelta agonists are exercise mimetics. Cell *134*, 405–415.

Ohno, H., Shinoda, K., Spiegelman, B.M., and Kajimura, S. (2012). PPARγ agonists induce a white-to-brown fat conversion through stabilization of PRDM16 protein. Cell Metab. *15*, 395–404.

Rance, N.E., Dacks, P.A., Mittelman-Smith, M.A., Romanovsky, A.A., and Krajewski-Hall, S.J. (2013). Modulation of body temperature and LH secretion by hypothalamic KNDy (kisspeptin, neurokinin B and dynorphin) neurons: a novel hypothesis on the mechanism of hot flushes. Front. Neuroendocrinol. *34*, 211–227.

Roa, J., Vigo, E., Castellano, J.M., Gaytan, F., Navarro, V.M., Aguilar, E., Dijcks, F.A., Ederveen, A.G., Pinilla, L., van Noort, P.I., and Tena-Sempere, M. (2008). Opposite roles of estrogen receptor (ER)-alpha and ERbeta in the modulation of luteinizing hormone responses to kisspeptin in the female rat: implications for the generation of the preovulatory surge. Endocrinology *149*, 1627–1637.

Roa, J., García-Galiano, D., Varela, L., Sánchez-Garrido, M.A., Pineda, R., Castellano, J.M., Ruíz-Pino, F., Romero, M., Aguilar, E., López, M., et al. (2009). The mammalian target of rapamycin as novel central regulator of puberty onset via modulation of hypothalamic Kiss1 system. Endocrinology *150*, 5016–5026.

Rogers, N.H., Perfield, J.W., 2nd, Strissel, K.J., Obin, M.S., and Greenberg, A.S. (2009). Reduced energy expenditure and increased inflammation are early events in the development of ovariectomy-induced obesity. Endocrinology *150*, 2161–2168.

Sánchez-Criado, J.E., Martín De Las Mulas, J., Bellido, C., Tena-Sempere, M., Aguilar, R., and Blanco, A. (2004). Biological role of pituitary estrogen receptors ERalpha and ERbeta on progesterone receptor expression and action and on gonadotropin and prolactin secretion in the rat. Neuroendocrinology *79*, 247–258.

Sánchez-Criado, J.E., de Las Mulas, J.M., Bellido, C., Navarro, V.M., Aguilar, R., Garrido-Gracia, J.C., Malagón, M.M., Tena-Sempere, M., and Blanco, A. (2006). Gonadotropin-secreting cells in ovariectomized rats treated with different oestrogen receptor ligands: a modulatory role for ERbeta in the gonadotrope? J. Endocrinol. *188*, 167–177.

Schneeberger, M., Dietrich, M.O., Sebastián, D., Imbernón, M., Castaño, C., Garcia, A., Esteban, Y., Gonzalez-Franquesa, A., Rodríguez, I.C., Bortolozzi, A., et al. (2013). Mitofusin 2 in POMC neurons connects ER stress with leptin resistance and energy imbalance. Cell *155*, 172–187.

Shibata, M., Uno, T., and Hashimoto, M. (1999). Neurons in the lower midbrain tonically inhibit non-shivering thermogenesis through their influence on inferior olivary neurons in anesthetized rats. J. Therm. Biol. *24*, 365–368.

Shughrue, P.J., Lane, M.V., and Merchenthaler, I. (1997). Comparative distribution of estrogen receptor-alpha and -beta mRNA in the rat central nervous system. J. Comp. Neurol. *388*, 507–525.

Sun, J., Huang, Y.R., Harrington, W.R., Sheng, S., Katzenellenbogen, J.A., and Katzenellenbogen, B.S. (2002). Antagonists selective for estrogen receptor alpha. Endocrinology *143*, 941–947.

Tritos, N.A., Segal-Lieberman, G., Vezeridis, P.S., and Maratos-Flier, E. (2004). Estradiol-induced anorexia is independent of leptin and melanin-concentrating hormone. Obes. Res. *12*, 716–724.

Uno, T., and Shibata, M. (2001). Role of inferior olive and thoracic IML neurons in nonshivering thermogenesis in rats. Am. J. Physiol. Regul. Integr. Comp. Physiol. *280*, R536–R546.

Vigo, E., Roa, J., López, M., Castellano, J.M., Fernandez-Fernandez, R., Navarro, V.M., Pineda, R., Aguilar, E., Diéguez, C., Pinilla, L., and Tena-Sempere, M. (2007). Neuromedin s as novel putative regulator of luteinizing hormone secretion. Endocrinology *148*, 813–823.

Waldén, T.B., Hansen, I.R., Timmons, J.A., Cannon, B., and Nedergaard, J. (2012). Recruited vs. nonrecruited molecular signatures of brown, "brite," and white adipose tissues. Am. J. Physiol. Endocrinol. Metab. *302*, E19–E31.

Welsh, J.P., and Llinás, R. (1997). Some organizing principles for the control of movement based on olivocerebellar physiology. Prog. Brain Res. *114*, 449–461.

Whittle, A.J., Carobbio, S., Martíns, L., Slawik, M., Hondares, E., Vázquez, M.J., Morgan, D., Csikasz, R.I., Gallego, R., Rodriguez-Cuenca, S., et al. (2012). BMP8B increases brown adipose tissue thermogenesis through both central and peripheral actions. Cell *149*, 871–885.

Williams, K.W., and Elmquist, J.K. (2012). From neuroanatomy to behavior: central integration of peripheral signals regulating feeding behavior. Nat. Neurosci. *15*, 1350–1355.

Wren, B.G. (2009). The benefits of oestrogen following menopause: why hormone replacement therapy should be offered to postmenopausal women. Med. J. Aust. *190*, 321–325.

Xu, Y., Nedungadi, T.P., Zhu, L., Sobhani, N., Irani, B.G., Davis, K.E., Zhang, X., Zou, F., Gent, L.M., Hahner, L.D., et al. (2011). Distinct hypothalamic neurons mediate estrogenic effects on energy homeostasis and reproduction. Cell Metab. *14*, 453–465.

Yeo, G.S., and Heisler, L.K. (2012). Unraveling the brain regulation of appetite: lessons from genetics. Nat. Neurosci. *15*, 1343–1349.

**Cell Metabolism, Volume *20***

## Supplemental Information

# Estradiol Regulates Brown Adipose Tissue Thermogenesis via Hypothalamic AMPK

**Pablo B. Martínez de Morentin, Ismael González-García, Luís Martins, Ricardo Lage, Diana Fernández-Mallo, Noelia Martínez-Sánchez, Francisco Ruíz-Pino, Ji Liu, Donald A. Morgan, Leonor Pinilla, Rosalía Gallego, Asish K. Saha,0 Andries Kalsbeek, Eric Fliers, Peter H. Bisschop, Carlos Diéguez, Rubén Nogueiras, Kamal Rahmouni, Manuel Tena-Sempere, and Miguel López**

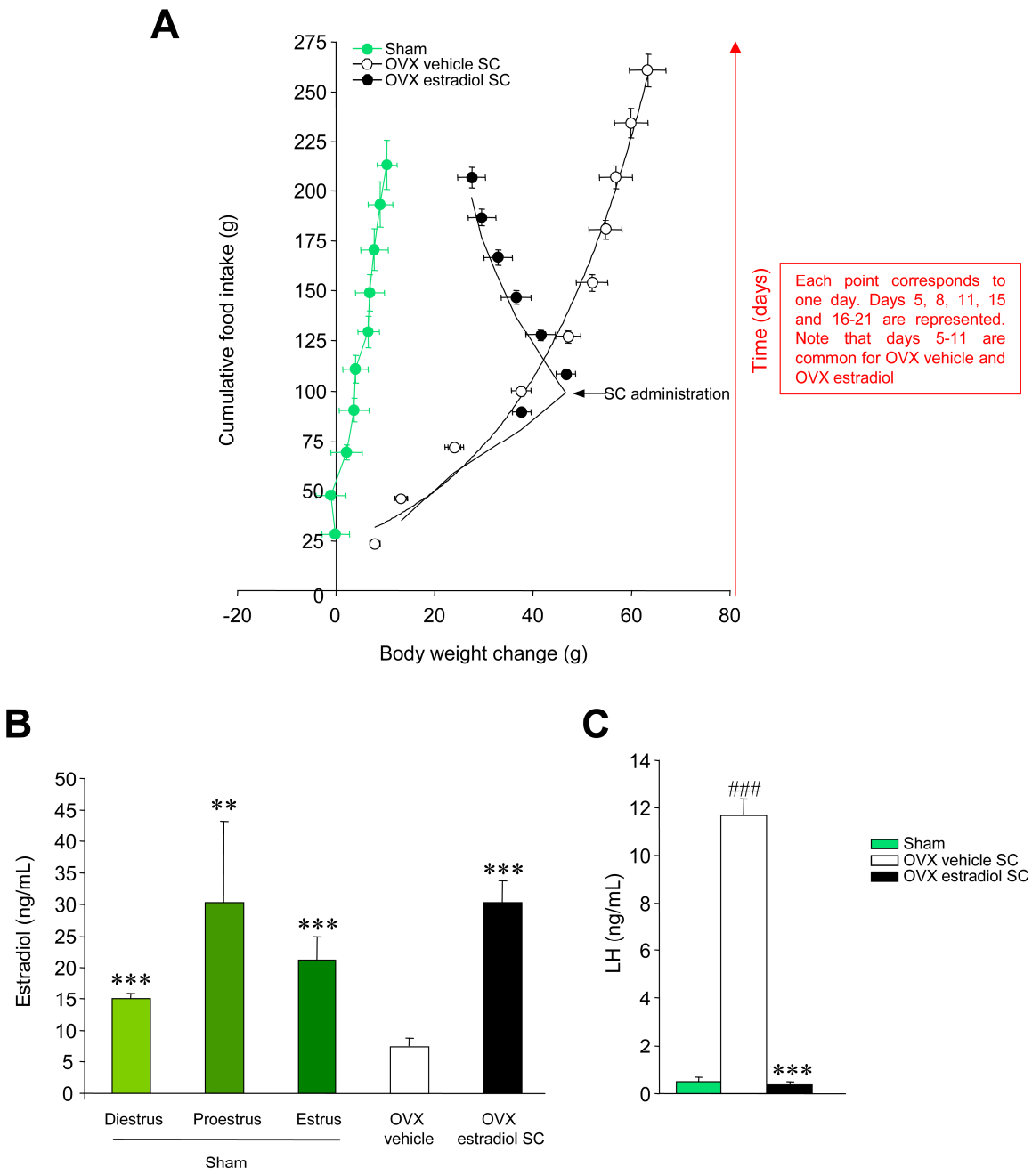


**FIGURE S1, related to Figure 1. Effect of peripheral E2 treatment on energy balance and plasma E2 and LH levels.**

**(A)** Energy balance plot, **(B)** plasma E2 levels (for sham rats in different stages of the estrus cycle) and **(C)** plasma luteinizing hormone (LH) levels of sham and OVX rats SC treated with vehicle or E2. Error bars represent SEM; n= 7-19 animals per experimental group. ** and ***P<0.01 and 0.001 *vs.* OVX E2 SC; ###P<0.001 *vs.* sham.

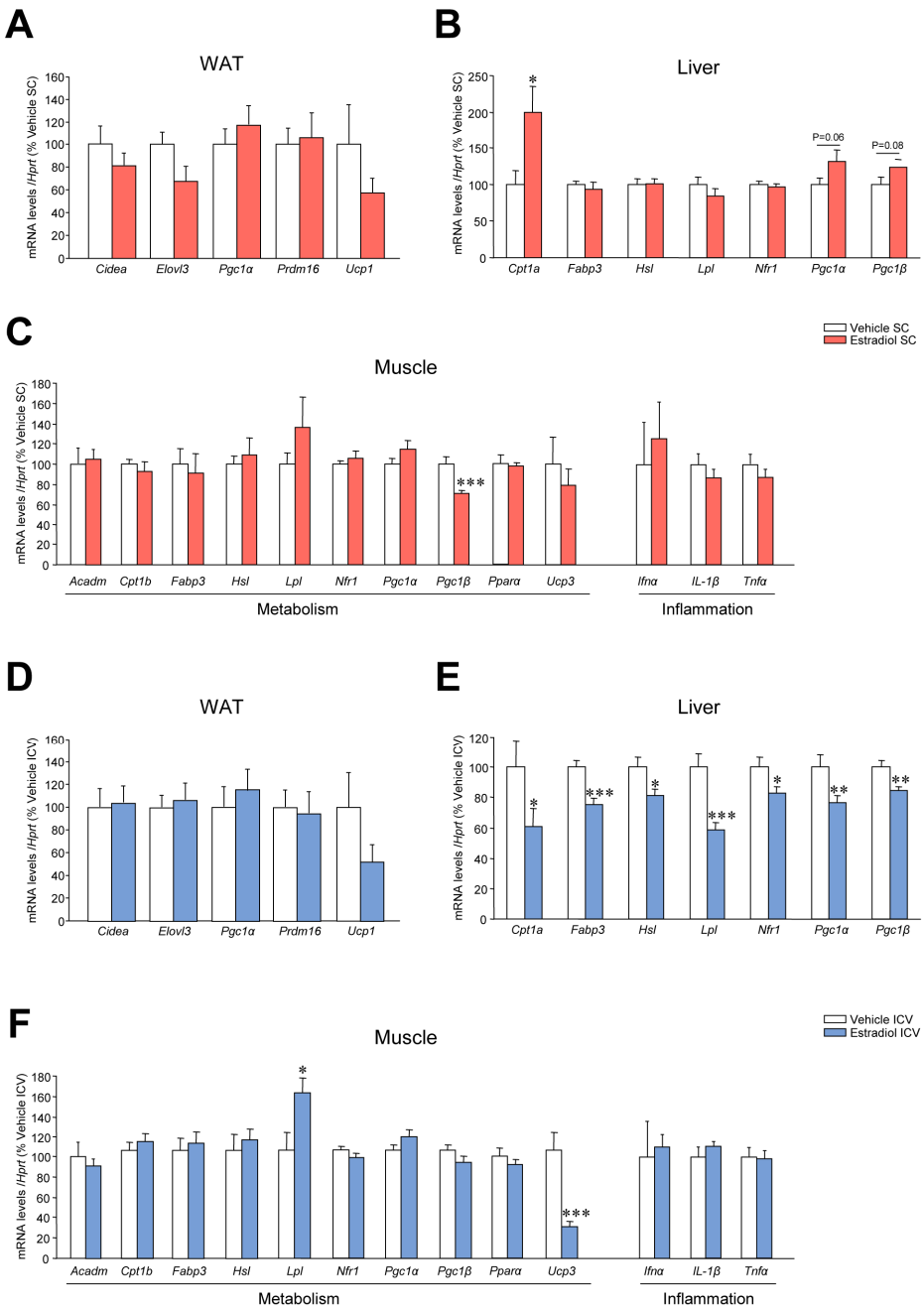


**FIGURE S2, related to Figure 2. Effect of peripheral or central E2 treatment on browning markers in WAT and metabolic and inflammatory markers in liver and muscle.**
mRNA profiles in WAT **(A)**, liver **(B)** and muscle **(C)** of OVX rats treated SC with vehicle or E2. mRNA profiles in WAT **(D)**, liver **(E)** and muscle **(F)** of OVX rats treated ICV with vehicle or E2. Error bars represent SEM; n= 7-9 animals per experimental group. *, ** and ***P<0.05, 0.01 and 0.001 *vs.* vehicle (SC or ICV).

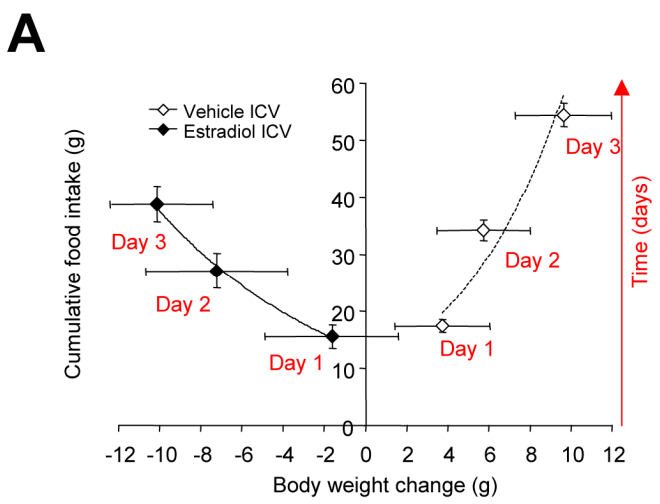


**FIGURE S3, related to Figure 3. Effect or central E2 treatment on energy balance.**
**(A)** Energy balance plot of rats treated with vehicle or E2. Error bars represent SEM; n= 12 animals per experimental group.

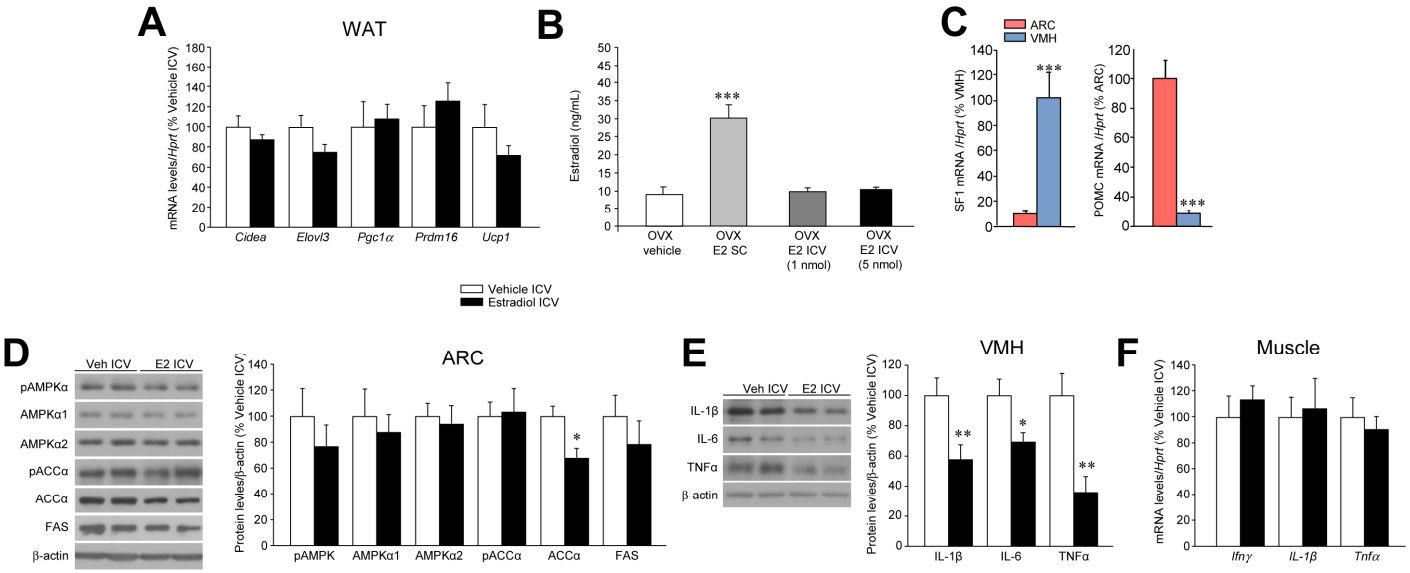


**FIGURE S4, related to Figure 4. Effect of central E2 treatment on WAT browning program, ARC AMPK pathway and hypothalamic and muscle inflammation.**

**(A)** Browning markers in WAT of OVX rats ICV treated with vehicle or E2. **(B)** Plasma E2 levels of OVX rats SC and ICV treated with vehicle or E2. **(C)** SF1 and POMC mRNA levels in VMH and ARC dissections. **(D)** Western blot autoradiographic images (left panel) and protein levels of the AMPK pathway in the ARC (right panel) of OVX rats ICV treated with vehicle or E2. **(E)** Western blot autoradiographic images (left panel) and protein levels of inflammatory markers (right panel) in the VMH of rats ICV treated with vehicle or E2. **(F)** mRNA levels of inflammatory markers in muscle of OVX rats ICV treated with vehicle or E2. Error bars represent SEM; n=7-19 animals per experimental group. *, ** and ***P<0.05, 0.01 and 0.001 *vs.* vehicle ICV.

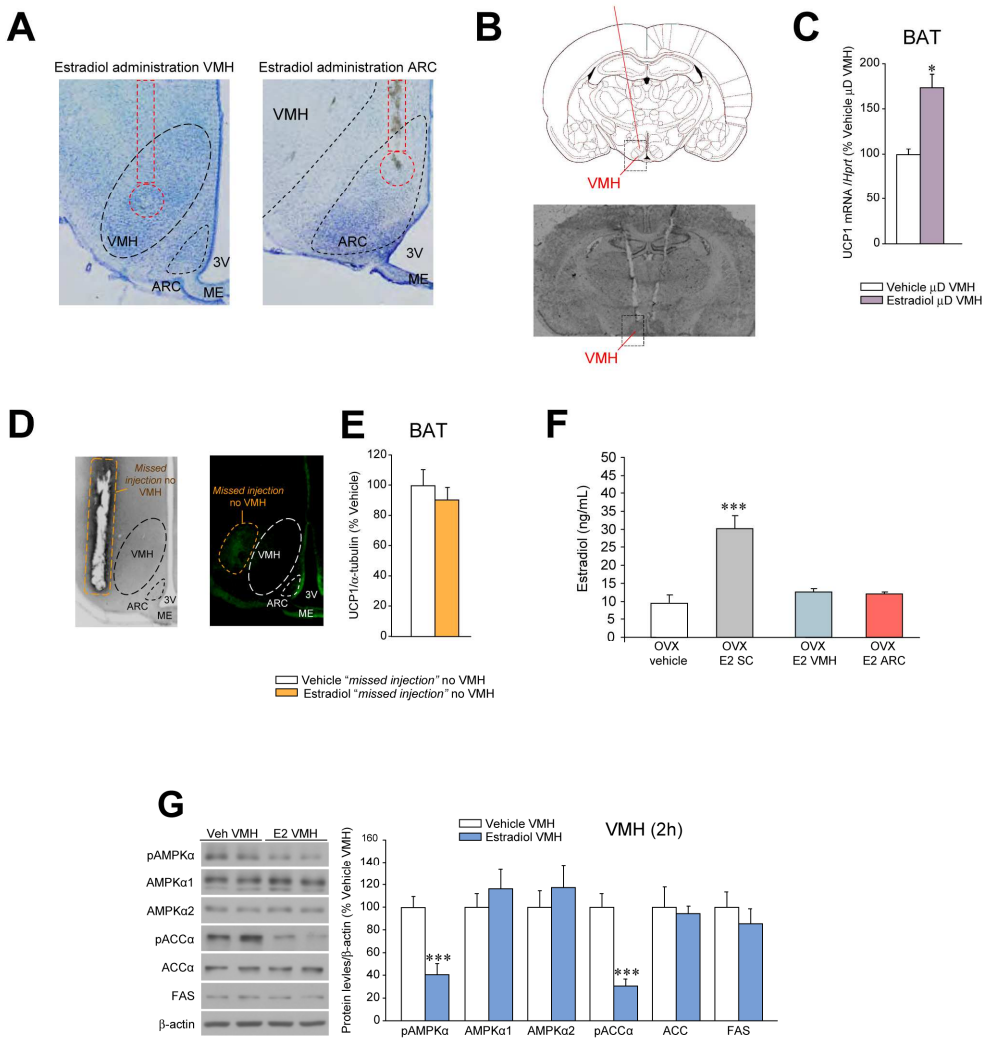


**FIGURE S5, related to Figure 5. Histological and expression controls of E2 administration into the VMH.**

**(A)** Representative photomicrographs (10X) of toluidine blue staining of brain sections from rats treated with E2 in the VMH or the ARC. The injection route is enclosed in a red rectangle and the injection place in a red circle. **(B)** Schematic representation (from *Paxinos and Watson Rat Brain Atlas;* upper panel) and representative photomicrograph of brain sections showing the injection route for microdialysis (lower panel) and **(C)** UCP1 mRNA levels in BAT of OVX rats treated by microdialysis with vehicle or E2 within the VMH. **(D)** Representative photomicrographs of brain sections (4X) showing *"missed"* injections in *"VMH neighboring"* areas in OVX rats. **(E)** BAT UCP1 protein levels of OVX rats with *"missed"* injections in *"VMH neighboring"* areas. **(F)** Plasma E2 levels of OVX rats SC, VMH or ARC treated with E2. **(G)** Western blot autoradiographic images (left panel) and protein levels of the AMPK pathway in the VMH (right panel) of OVX rats stereotaxically treated with vehicle or E2 within the VMH for 2 hours. Error bars represent SEM; n=6-19 animals per experimental group. *P<0.05 *vs.* vehicle µD VMH and ***P<0.001 *vs.* OVX vehicle or vehicle VMH.

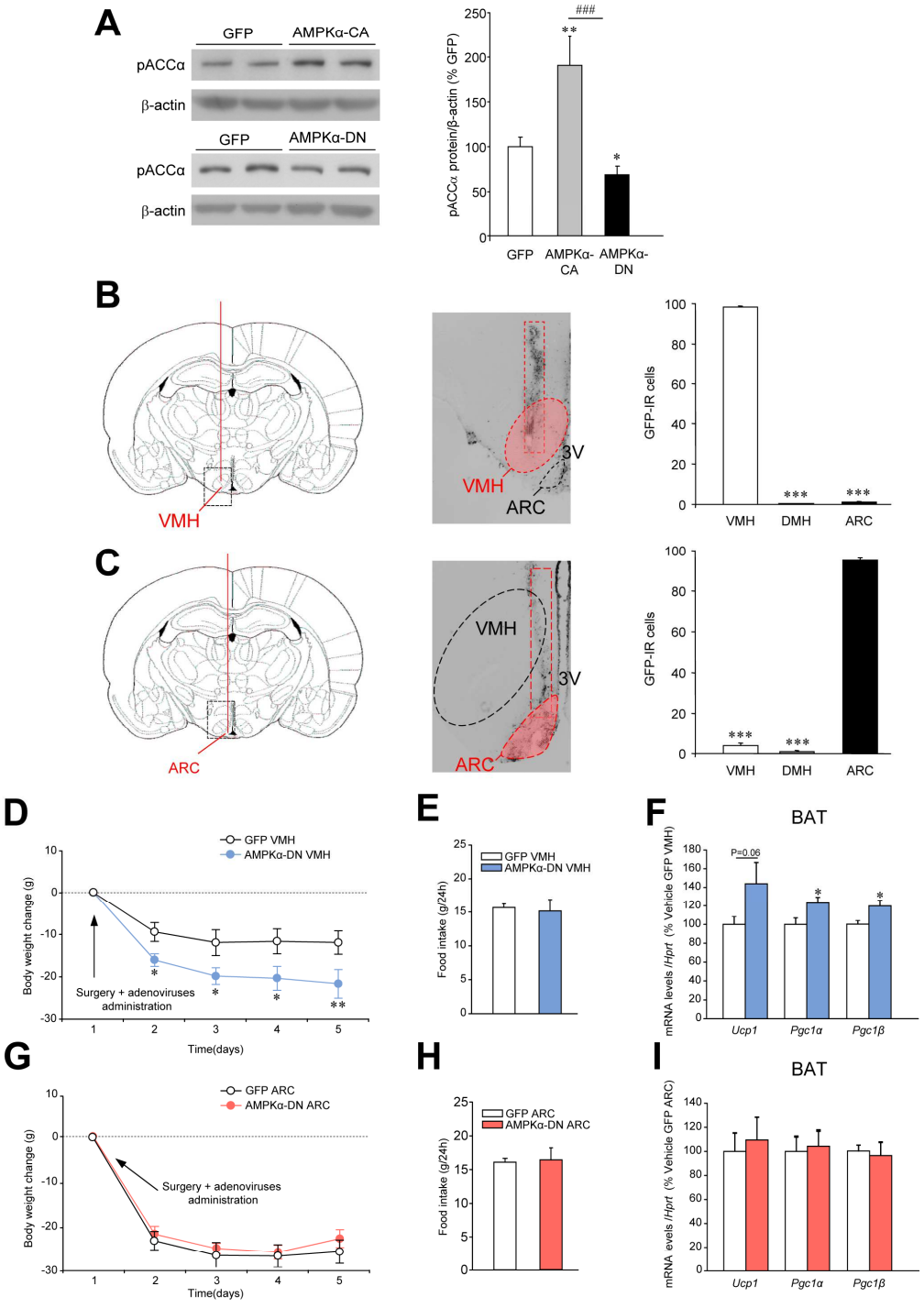


**FIGURE S6, related to Figure 6. Histological and expression controls of AMPKα adenoviruses administration into the VMH and ARC. Effect of inactivation of hypothalamic AMPK in OVX rats on energy balance.**

**(A)** Western blot autoradiographic images (left panel) and hypothalamic protein levels of pACCα (right panel) of rats stereotaxically treated with adenoviruses encoding GFP, AMPKα-CA and AMPKα-DN. **(B)** Schematic representation (from *Paxinos and Watson Rat Brain Atlas,* left panel), representative photomicrograph of brain sections (central panel) showing the injection route for stereotaxic administration and GFP-immunopositive cells (right panel) of rats treated with AMPKα adenoviruses into the VMH. **(C)** Schematic representation (from *Paxinos and Watson Rat Brain Atlas,* left panel), representative photomicrograph (central panel) showing the injection route for stereotaxic

administration and GFP-immunopositive cells (right panel) of rats treated with AMPKα adenoviruses into the ARC. **(D)** Body weight, **(E)** daily food intake and **(F)** mRNA expression profile in the BAT of OVX rats stereotaxically treated with GFP or AMPKα-DN adenoviruses into the VMH. **(G)** Body weight, **(H)** daily food intake and **(I)** mRNA expression profile in the BAT of OVX rats stereotaxically treated with GFP or AMPKα-DN adenoviruses into the ARC. Error bars represent SEM; n= 8 animals per experimental group. 3V: third ventricle; *P<0.05 *vs.* GFP or GFP VMH; **P<0.01 *vs.* GFP; ***P<0.001 *vs.* VMH or ARC (panels B and C); ###P<0.01 *vs.* AMPKα-DN

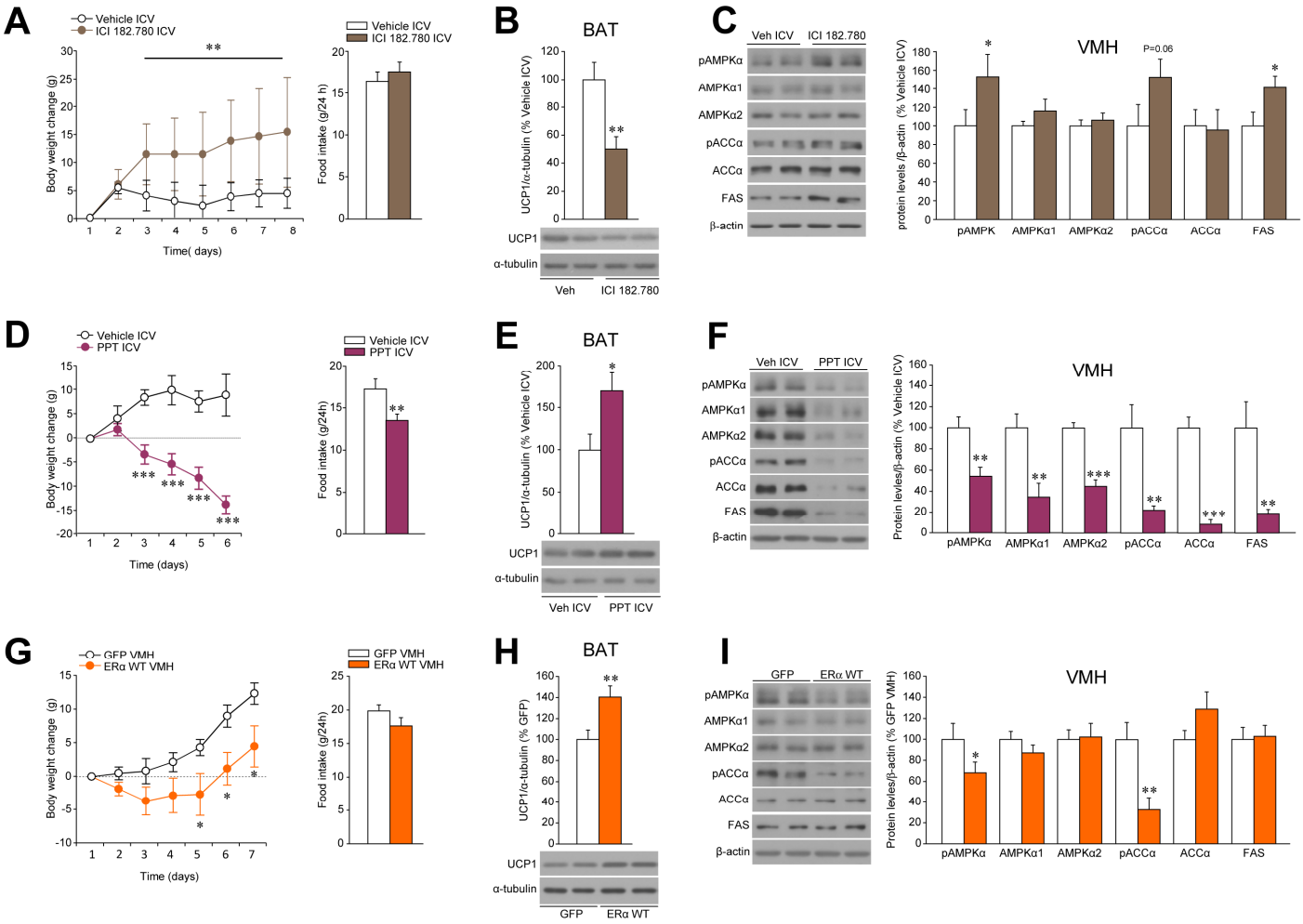


**FIGURE S7, related to Figure 7. Effect of pharmacological and genetic modulation of estrogen receptor alpha (ERα) over energy balance.**
**(A)** Body weight change (left panel) and daily food intake (right panel), **(B)** protein levels (upper panel) and western blot autoradiographic images of BAT UCP1 protein (lower panel) and **(C)** western blot autoradiographic images (left panel) and protein levels of the AMPK pathway in the VMH (right panel) of intact rats ICV treated with the combined ERα-β antagonist ICI 182.780. **(D)** Body weight change (left panel) and daily food intake (right panel), **(E)** protein levels (upper panel) and western blot autoradiographic images of BAT UCP1 protein (lower panel) and **(F)** western blot autoradiographic images (left panel) and protein levels of the AMPK pathway in the VMH (right panel) of OVX rats ICV treated with the specific ERα agonist PPT. **(G)** Body weight change (left panel) and daily food intake (right panel), **(H)** protein levels (upper panel) and western blot autoradiographic images of BAT UCP1 protein (lower panel) and **(I)** western blot autoradiographic images (left panel) and protein levels of the AMPK pathway in the VMH (right panel) of OVX rats stereotaxically treated within the VMH with adenovirus encoding a wildtype (WT) isoform of ERα. Error bars represent SEM; n=7-8 animals per experimental group. *, ** and *** P<0.05, 0.01 and 0.001 *vs.* vehicle ICV or GFP VMH.

**Table S1:** Primers and probes for real-time PCR analysis

| *mRNA* | Gene name | GenBank Accession number | | Sequence |
|---|---|---|---|---|
| *Acadm* | Acyl-CoA dehydrogenase | NM_016986.2 | Fw Primer | 5'-GCCTTCACCGGATTCATCGT-3' |
| | | | Rv Primer | 5'-GCACCGCTGACCCATGTT-3' |
| | | | Probe | 5'-FAM-CCCGGGAATACACATCGGAAAAAAGGAACT-3' |
| *Cidea* | Cell death-inducing DFFA-like effector a | NM_001170467.1 | Assay ID | Applied Biosystems TaqMan® Gene Expression Assays Assay ID Rn04181355_m1 |
| *Cpt1a* | Carnitine palmitoyltransferase 1a, (liver) | NM_031559.1 | Fw Primer | 5´-ATGACGGCTATGGTGTCTCC-3 |
| | | | Rv Primer | 5´-TCATGGCTTGCTTCAAGTGC-3´ |
| | | | Probe | FAM-5´-TGAGACAGACTCACACCGCT-3´-TAMRA |
| *Cpt1b* | Carnitine palmitoyltransferase 1b, (muscle) | NM_013200 | Assay ID | Applied Biosystems TaqMan® Gene Expression Assays Assay ID Rn01407782_g1 |
| *Elovl3* | Fatty acid elongase 3 | NM_001107602.1 | Assay ID | Applied Biosystems TaqMan® Gene Expression Assays Assay ID Rn01411024_m1 |
| *Fabp3* | Fatty acid binding protein 3 | NM_024162 | Fw Primer | 5'-ACGGAGGCAAACTGGTCCAT-3' |
| | | | Rv Primer | 5'-CACTTAGTTCCCGTGTAAGCGTAGTC-3' |
| | | | Probe | FAM-5'-TGCAGAAGTGGGACGGGCAGG-3'-TAMRA |
| *Hprt* | Hypoxanthine phosphoribosyltransferase 1 | NM_012583 | Fw Primer | 5'-AGCCGACCGGTTCTGTCAT-3' |
| | | | Rv Primer | 5'-GGTCATAACCTGGTTCATCATCAC -3' |
| | | | Probe | FAM-5'- CGACCCTCAGTCCCAGCGTCGTGAT 3'-TAMRA |
| *Hsl* | Lpase, hormone sensitive (Lipe) | NM_012859 | Fw Primer | 5'-CCAAGTGTGTGAGCGCCTATT -3' |
| | | | Rv Primer | 5'-TCACGCCCAATGCCTTCT -3' |
| | | | Probe | FAM-5'-AGGGACAGAGACGGAGGACCATTTTGACTC -3'-TAMRA |
| *Ifnγ* | Interferon gamma | NM_138880.2 | Assay ID | Applied Biosystems TaqMan® Gene Expression Assays Assay ID Rn00594078_m1 |
| *Il-1β* | Interleukin 1 beta | NM_031512.2 | Assay ID | Applied Biosystems TaqMan® Gene Expression Assays Assay ID Rn00580432 |
| *Lpl* | Lipoprotein lipase | NM_012598 | Fw Primer | 5'-CTGAAAGTGAGAACATTCCCTTCA-3' |
| | | | Rv Primer | 5'-CCGTGTAAATCAAGAAGGAGTAGGTT-3' |
| | | | Probe | FAM-5'-CCTGCCGGAGGTCGCCACAAATA-3'-TAMRA |
| *Nrf-1* | Nuclear respiratory factor 1 | NM_001100708.1 | Fw Primer | 5´-TGTTTGGCGCAGCACCTTT-3´ |
| | | | Rv Primer | 5´-CGC AGA CTC CAG GTC TTC CA-3´ |
| | | | Probe | FAM-5´-ATGTGGTGCGCAAGTACAAGAGCATGATC3´- |

| | | | | |
|---|---|---|---|---|
| | | | | TAMRA |
| *Pdrm16* | PR domain containing 16 | NM_001177995.1 | Assay ID | Applied Biosystems TaqMan® Gene Expression Assays<br>Assay ID Mm01266512_m1 |
| *Pgc1α* | Peroxisome proliferator-activated receptor gamma, coactivator 1 alpha (Ppargc1a) | NM_031347 | Fw Primer | 5’-CGATCACCATATTCCAGGTCAAG-3’ |
| | | | Rv Primer | 5’-CGATGTGTGCGGTGTCTGTAGT -3’ |
| | | | Probe | 5’-AGGTCCCCAGGCAGTAGATCCTCTTCAAGA -3’ |
| *Pgc1β* | Peroxisome proliferator-activated receptor gamma, coactivator 1 beta (Ppargc1b) | NM_176075 | Assay ID | Applied Biosystems TaqMan® Gene Expression Assays<br>Assay ID Rn00598552_m1 |
| *Pomc* | Proopiomelanocortin | | Fw Primer | 5’-CGTCCTCAGAGAGCTGCCTTT-3’ |
| | | | Rv Primer | 5’-TGTAGCAGAATCTCGGCATCTTC-3’ |
| | | | Probe | FAM-5’-CGCGACAGAGCCTCAGCCACC-3’-TAM |
| *Pparα* | Peroxisome proliferator activated receptor alpha | NM_013196.1 | Fw Primer | 5’-TGGAGTCCACGCATGTGAAG-3’ |
| | | | Rv Primer | 5’-CGCCAGCTTTAGCCGAATAG-3’ |
| | | | Probe | 5’-FAM-CTGCAAGGGCTTCTTTCGGCGA-3’ |
| *Ucp1* | Uncoupling protein 1 | NM_012682 | Fw Primer | 5’-CAATGACCATGTACACCAAGGAA-3' |
| | | | Rv Primer | 5’-GATCCGAGTCGCAGAAAAGAA-3' |
| | | | Probe | FAM-5’-ACCGGCAGCCTTTTTCAAAGGGTTTG-3’-TAMRA |
| | | | Fw Primer | 5’-AATCAGCTTTGCTTCCCTCA-3’ |
| | | | Rv Primer | 5’-GCT TTGTGCTTGCATTCTGA-3' |
| | | | SYBR green | |
| *Ucp3* | Uncoupling protein 3 | NM_013167.2 | Assay ID | Applied Biosystems TaqMan® Gene Expression Assays<br>Assay ID Rn00565874_m1 |
| *Sf-1* | Steroidogenic factor 1 | | Assay ID | Applied Biosystems TaqMan® Gene Expression Assays<br>Assay ID Rn00584298_m1 |
| *Tnfα* | Tumor necrosis factor alpha | NM_012675.3 | Fw Primer | 5’-CTAACTCCCAGAAAAGCAAGCAA-3’ |
| | | | Rv Primer | 5’-CCTCGGGCCAGTGTATGAGA-3’ |
| | | | Probe | 5’-FAM-CAGCCAGGCAGGTTCCGTCC-3’ |

## SUPPLEMENTAL EXPERIMENTAL PROCEDURES

### Determination of estrus cycle stages

Female rats were monitored for estrus cycle by daily vaginal cytology, and only rats with at least two consecutive regular 4-days estrus cycles were used in expression analyses, as previously reported (Vigo et al., 2007).

### Implantation of intracerebroventricular cannulae

Chronic intracerebroventricular (ICV) cannulae were implanted under ketamine/xylacine anesthesia, as described previously and correct positioning in the lateral ventricle was confirm by postmortem histological examination (López et al., 2008; López et al., 2010; Martínez de Morentin et al., 2012; Whittle et al., 2012). The animals were caged individually and used for experimentation four days later. During this post-operative recovery period the rats became accustomed to the handling procedure under non-stressful conditions.

### Implantation of microdialysis probes and central treatments

Rats were placed in a stereotaxic frame (*David Kopf Instruments;* Tujunga, CA, USA) under ketamine/xylazine anesthesia. Bilateral microdialysis probes were placed in the VMH as previously reported (Liu et al., 2013). The coordinates for the ICV probe were AP: 0.6mm, lateral: 1.5mm and ventral 3.5mm from the surface of the dura and for the VMH AP: 2.5mm, lateral: 2.0mm (angled at 10°) and 9.0 mm ventral from the dura. Microdialysis probes were implanted 1-week before the start of the experiment. The day before the experiment animals were connected to a metal collar which was kept out of reach from the rats by means of a counterbalanced beam. This allowed all manipulations to be performed outside the cages without handling the animals. 1 mg of 17β-estradiol

(17β-E2; *Sigma;*, St. Louis, MO, USA) was dissolved in 1 ml pure DMSO and diluted 100 times with Ringer solution. Ringer's dialysis (3µl/min) in the VMH via the microdialysis probes was started at t=-60 min. At t=0 min 17β-E2 (10 µg/ml, 3 µl/min) or vehicle (Ringer with 1% DMSO, 3 µl/min) were infused by retrodialysis into VMH during a period of 180 min.

**Stereotaxic microinjection**

Rats treated with vehicle or E2 were placed in a stereotaxic frame (*David Kopf Instruments;* Tujunga, CA, USA) under ketamine/xylazine anesthesia. The ARC and the VMH were targeted bilaterally using a 25-gauge needle (*Hamilton;* Reno, NV, USA). The injections were directed to the following stereotaxic coordinates: *a)* for the VMH: 2.4/3.2 mm posterior to the bregma (two injections were performed in each VMH), ±0.6 mm lateral to midline and 10.1 mm ventral; *b)* for the ARC -2.8 mm posterior (one injection was performed in each ARC), ±0.3 mm lateral to bregma and 10.2 mm ventral, as previously reported (López et al., 2008; López et al., 2010; Martínez de Morentin et al., 2012; Whittle et al., 2012). Viral vectors were delivered at a rate of 200 nl/min for 5 min (1 µl/injection site) as previously reported (López et al., 2008; López et al., 2010; Martínez de Morentin et al., 2012; Whittle et al., 2012).

**Sample processing**

In central treatments with E2 (ICV. ARC and VMH) animals were treated at 09:00 AM (one hour after the light cycle had commenced). Rats were killed by cervical dislocation. From each animal, the blood (for hormonal measurements), the whole hypothalamus, MBH, ARC, VMH, BAT, WAT, liver and muscle (for western blotting or malonyl-CoA assays) were immediately homogenized on ice to preserve

phosphorylated protein levels or the whole brain (for *in situ* hybridization) was dissected, and stored at -80ºC until further processing. Dissection of the ARC and VMH was performed by micropunches under the microscope, as previously shown (López et al., 2010; Varela et al., 2012). The specificity of the ARC and VMH dissection was confirmed by analyzing the mRNA of their specific markers, namely SF1 and POMC **(Supplementary Figure 4A).**

**Energy expenditure, locomotor activity, respiratory quotient, lipid utilization and nuclear magnetic resonance analysis**

Rats were analyzed for energy expenditure (EE), respiratory quotient (RQ) and locomotor activity (LA) using a calorimetric system (*LabMaster; TSE Systems;* Bad Homburg, Germany), as previously shown (Nogueiras et al., 2007; Martínez de Morentin et al., 2012; Imbernon et al., 2013). Rats were placed for adaptation for 1 week before starting the measurements. For the measurement of body composition, we used the nuclear magnetic resonance **(**NMR) imaging (*Whole Body Composition Analyzer; EchoMRI;* Houston, TX), as previously shown (López et al., 2010; Martínez de Morentin et al., 2012; Imbernon et al., 2013).

**Sympathetic nerve activity recording**

Multi-fiber recording of sympathetic nerve activity (SNA) was obtained from the nerve subserving BAT, as previously described (Rahmouni et al., 2004; López et al., 2010; Whittle et al., 2012; Imbernon et al., 2013). Briefly, anesthesia was induced with ketamine/xylazine (91/9.1 mg/kg) and sustained with intravenous administration of α-chloralose (initial dose: 25 mg/kg; sustaining dose of 6mg/kg/h). Each rat, equipped with ICV cannula 1 week earlier, was intubated (PE-50) to allow for spontaneous

respiration of oxygen-enriched room air. Body temperature was kept constant at 37.5$^{o}$ C with a surgical heat lamp and a heat pad to ensure that the preparation is stable. The nerve subserving BAT was identified using a dissecting scope and then mounted on a bipolar 36-gauge platinum-iridium electrode (*Cooner Wire Co.*, Chadsworth, CA, US). The nerve electrodes were attached to a high-impedance probe (*HIP-511, Grass Instruments Co.*, Quincy, Ma, US). The signal was amplified $10^5$ times with a Grass P5 AC preamplifier, and filtered at both low (100Hz) and high-frequency (1000Hz) cut-off. This amplified, filtered signal was then sent to a speaker system and oscilloscope (*Model 54501A, Hewlett-Packard Co.*, Palo Alto, Ca. US). The signal was also routed to a *MacLab* analogue-digital converter (*Model 8S, Ad Instruments*, Castle Hill, New South Wales, Australia) for a permanent recording and data analysis on a *Macintosh* computer. Baseline BAT SNA was measured during a 10 min control period before a bolus ICV injection of vehicle or E2 was performed. The BAT SNA response to vehicle or E2 was followed for 6 hours. Background noise was excluded in the assessments of BAT SNA by correcting for post-mortem activity. SNA was expressed as a percent change from baseline.

**Temperature measurements**

Body temperature was recorded twice at the end of the treatments with a rectal probe connected to digital thermometer (*BAT-12 Microprobe-Thermometer; Physitemp*; NJ, US). Skin temperature surrounding BAT was recorded with an infrared camera (*E60bx: Compact-Infrared-Thermal-Imaging-Camera; FLIR;* West Malling, Kent, UK) and analyzed with a specific software package (*FLIR-Tools-Software; FLIR;* West Malling, Kent, UK) (Martínez de Morentin et al., 2012; Whittle et al., 2012;

Schneeberger et al., 2013). The skin temperature surrounding BAT for each particular animal was calculated as the average temperature recorded by analyzing 6 pictures.

**Hormone measurements**

Absence of gonadal function was confirmed by increased LH serum levels measured using a double-antibody method and radioimmunoassay kits (supplied by *Dr. AF Parlow; National Institute of Diabetes and Digestive and Kidney Diseases National Hormone and Peptide Program;,* Torrance, CA) as reported (Vigo et al., 2007; Roa et al., 2009). Rat LH-I-10 was labeled in-house with 125I using *Iodo-gen® tubes* (*Pierce;* Rockford, IL, US). Hormone concentrations were expressed using the reference preparation LH-RP-3. The intra- and inter-assay coefficients of variation (CVs) were <8% and <10%, respectively. Circulating E2 levels were determined using a commercial ultra-sensitive RIA kit (*Beckman Coulter;* Brea, CA, US). The sensitivity of the assay was 2.2 pg/mL, and the intra- and inter-assay CVs were 8.9% and 12.2%, respectively.

**Malonyl-CoA assay**

The malonyl-CoA assays were performed as described (López et al., 2006; López et al., 2008; López et al., 2010).

**Real-time quantitative PCR**

Real-time PCR (*TaqMan®, Applied Biosystems*; Foster City, CA, USA; or *SYBR® Green, Roche Molecular Biochemicals,* Mannheim, Germany, for the BAT samples form the microdialysis experiments) was performed using specific primers and probes **(Table S1)** as previously described (López et al., 2010; Martínez de Morentin et

al., 2012; Whittle et al., 2012). Values were expressed in relation to hypoxanthine-guanine phosphoribosyl-transferase (HPRT) levels.

**In situ hybridization**

Coronal brain sections (16 µm) were probed with a specific oligonucleotide for NPY (*GenBank Accession Number*: M20373; 5'-AGA TGA GAT GTG GGG GGA AAC TAG GAA AAG TCA GGA GAG CAA GTT TCA TT-3') and POMC (*GenBank Accession Number*: AF510391; 5'-CTT GAT GAT GGC GTT CTT GAA GAG CGT CAC CAG GGG CGT CTG GCT CTT-3') as previously published (López et al., 2006; López et al., 2008; Lage et al., 2010; López et al., 2010; Martínez de Morentin et al., 2012; Varela et al., 2012; Whittle et al., 2012). Sections were scanned and the hybridization signal was quantified by densitometry using *ImageJ-1.33* (*NIH;* Bethesda, MD, USA). We used between 16-20 sections for each animal (4-5 slides with four sections per slide). The mean of these 16-20 values was used as the densitometry value for each animal.

**Western blotting**

Hypothalamic, ARC and VMH protein lysates were subjected to SDS-PAGE, electrotransferred on a PVDF membrane and probed with the following antibodies: ACC, pACC-Ser$^{79}$, AMPKα1, AMPKα2 (*Upstate;* Temecula, CA, USA); FAS (*BD*; Franklin Lakes, NJ, USA), AKT, pAKT-Ser$^{473}$, pAMPK-Thr$^{172}$, Il-1β, pLKB1-Ser$^{428}$, PI3K, pPI3K-Tyr$^{199}$, STAT3, TNFα (*Cell Signaling;* Danvers; MA, USA); α-tubulin, β-actin (*Sigma;* St. Louis, MO, USA), IL-6, UCP1, pSTAT3-Tyr$^{705}$ (*Abcam*; Cambridge, UK), CaMKKα, CaMKKβ, PP2Cα, (*Santa Cruz*; Santa Cruz, CA, USA) as previously described (López et al., 2006; López et al., 2008; Roa et al., 2009; Lage et al., 2010;

López et al., 2010; Martínez de Morentin et al., 2012; Varela et al., 2012; Whittle et al., 2012; Imbernon et al., 2013). Values were expressed in relation to α-tubulin (for BAT), β-actin (hypothalamus) protein levels.

**Immunohistochemistry**

Enzymatic immunohistochemistry (*Dako EnVision™+ system, peroxidase;* Glostrup, Denmark), immunofluorescence and double labeling were performed as described (López et al., 2008; López et al., 2010; Varela et al., 2012; Whittle et al., 2012), using a rabbit anti-c-FOS (*Santa Cruz Biotechnology*, CA, USA). c-FOS positive cells were counted by using *ImageJ-1.33* (*NIH*; Bethesda, MD, USA). Five animals per experimental group were used and 7-11 image sections were bilaterally analyzed per animal. Toluidine blue staining was performed as previously reported (Varela et al., 2012). Detection of GFP was performed with an immunofluorescence procedure, using a rabbit anti-GFP (1:200; *Abcam*; Cambridge, UK). Detection was done with an anti-rabbit antibody conjugated with *Alexa 488* (1:200; *Molecular Probes;* Grand Island, NY, US) as previously reported (López et al., 2008; López et al., 2010; Varela et al., 2012; Whittle et al., 2012; Imbernon et al., 2013).

## SUPPLEMENTAL REFERENCES


Imbernon, M., Beiroa, D., Vazquez, M.J., Morgan, D.A., Veyrat-Durebex, C., Porteiro, B., Diaz-Arteaga, A., Senra, A., Busquets, S., Velasquez, D.A., Al-Massadi, O., Varela, L., Gandara, M., Lopez-Soriano, F.J., Gallego, R., Seoane, L.M., Argiles, J.M., López, M., Davis, R.J., Sabio, G., Rohner-Jeanrenaud, F., Rahmouni, K., Diéguez, C., and Nogueiras, R. (2013). Central Melanin-Concentrating Hormone Influences Liver and Adipose Metabolism Via Specific Hypothalamic Nuclei and Efferent Autonomic/JNK1 Pathways. Gastroenterology *144*, 636-649.

Lage, R., Vázquez, M.J., Varela, L., Saha, A.K., Vidal-Puig, A., Nogueiras, R., Diéguez, C., and López, M. (2010). Ghrelin effects on neuropeptides in the rat hypothalamus depend on fatty acid metabolism actions on BSX but not on gender. FASEB J. *24*, 2670-2679.

Liu, J., Bisschop, P.H., Eggels, L., Foppen, E., Ackermans, M.T., Zhou, J.N., Fliers, E., and Kalsbeek, A. (2013). Intrahypothalamic estradiol regulates glucose metabolism via the sympathetic nervous system in female rats. Diabetes *62*, 435-443.

López, M., Lage, R., Saha, A.K., Pérez-Tilve, D., Vázquez, M.J., Varela, L., Sangiao-Alvarellos, S., Tovar, S., Raghay, K., Rodríguez-Cuenca, S., Deoliveira, R.M., Castañeda, T., Datta, R., Dong, J.Z., Culler, M., Sleeman, M.W., Álvarez, C.V., Gallego, R., Lelliott, C.J., Carling, D., Tschop, M.H., Diéguez, C., and Vidal-Puig, A. (2008). Hypothalamic fatty acid metabolism mediates the orexigenic action of ghrelin. Cell Metab *7*, 389-399.

López, M., Lelliott, C.J., Tovar, S., Kimber, W., Gallego, R., Virtue, S., Blount, M., Vázquez, M.J., Finer, N., Powles, T., O'Rahilly, S., Saha, A.K., Diéguez, C., and Vidal-Puig, A.J. (2006). Tamoxifen-induced anorexia is associated with fatty acid synthase inhibition in the ventromedial nucleus of the hypothalamus and accumulation of malonyl-CoA. Diabetes *55*, 1327-1336.

López, M., Varela, L., Vázquez, M.J., Rodríguez-Cuenca, S., González, C.R., Velagapudi, V.R., Morgan, D.A., Schoenmakers, E., Agassandian, K., Lage, R., de Morentin, P.B., Tovar, S., Nogueiras, R., Carling, D., Lelliott, C., Gallego, R., Oresic, M., Chatterjee, K., Saha, A.K., Rahmouni, K., Diéguez, C., and Vidal-Puig, A. (2010). Hypothalamic AMPK and fatty acid metabolism mediate thyroid regulation of energy balance. Nat. Med. *16*, 1001-1008.

Martínez de Morentin, P.B., Whittle, A.J., Ferno, J., Nogueiras, R., Diéguez C, Vidal-Puig, A., and López M (2012). Nicotine induces negative energy balance through hypothalamic AMP-activated protein kinase. Diabetes *61*, 807-817.

Nogueiras, R., Wiedmer, P., Perez-Tilve, D., Veyrat-Durebex, C., Keogh, J.M., Sutton, G.M., Pfluger, P.T., Castaneda, T.R., Neschen, S., Hofmann, S.M., Howles, P.N., Morgan, D.A., Benoit, S.C., Szanto, I., Schrott, B., Schurmann, A., Joost, H.G., Hammond, C., Hui, D.Y., Woods, S.C., Rahmouni, K., Butler, A.A., Farooqi, I.S., O'rahilly, S., Rohner-Jeanrenaud, F., and Tschop, M.H. (2007). The central melanocortin system directly controls peripheral lipid metabolism. J. Clin. Invest *117*, 3475-3488.

Rahmouni, K., Morgan, D.A., Morgan, G.M., Liu, X., Sigmund, C.D., Mark, A.L., and Haynes, W.G. (2004). Hypothalamic PI3K and MAPK differentially mediate regional sympathetic activation to insulin. J. Clin. Invest *114*, 652-658.

Roa, J., García-Galiano, D., Varela, L., Sánchez-Garrido, M.A., Pineda, R., Castellano, J.M., Ruíz-Pino, F., Romero, M., Aguilar, E., López, M., Gaytan, F., Diéguez, C., Pinilla, L., and Tena-Sempere, M. (2009). The mammalian target of rapamycin as novel central regulator of puberty onset via modulation of hypothalamic Kiss1 system. Endocrinology *150*, 5016-5026.

Schneeberger, M., Dietrich, M.O., Sebastian, D., Imbernon, M., Castano, C., Garcia, A., Esteban, Y., Gonzalez-Franquesa, A., Rodriguez, I.C., Bortolozzi, A., Garcia-Roves, P.M., Gomis, R., Nogueiras, R., Horvath, T.L., Zorzano, A., and Claret, M. (2013). Mitofusin 2 in POMC neurons connects ER stress with leptin resistance and energy imbalance. Cell *155*, 172-187.

Varela, L., Martínez-Sánchez N., Gallego, R., Vázquez, M.J., Roa, J., Gándara M., Schoenmakers, E., Nogueiras, R., Chatterjee, K., Tena-Sempere, M., Diéguez C, and López M (2012). Hypothalamic mTOR pathway mediates thyroid hormone-induced hyperphagia in hyperthyroidism. J. Pathol. *227*, 209-222.

Vigo, E., Roa, J., Lopez, M., Castellano, J.M., Fernandez-Fernandez, R., Navarro, V.M., Pineda, R., Aguilar, E., Dieguez, C., Pinilla, L., and Tena-Sempere, M. (2007). Neuromedin s as novel putative regulator of luteinizing hormone secretion. Endocrinology *148*, 813-823.

Whittle, A.J., Carobbio S, Martíns L, Slawik, M., Hondares, E., Vázquez, M.J., Morgan D, Csikasz, RI, Gallego, R., Rodriguez-Cuenca, S., Dale, M., Virtue, S., Villarroya, F., Cannon, B., Rahmouni, K., López M, and Vidal-Puig, A. (2012). Bmp8b increases brown adipose tissue thermogenesis through both central and peripheral actions. Cell *149*, 871-885.